AD_____
(Leave blank)

Award Number: W81XWH-08-1-0285

TITLE: DEVELOPMENT OF LEAD COMPOUNDS AS FUSION INHIBITORS FOR DENGUE VIRUS

PRINCIPAL INVESTIGATOR: TOMAS PEREZ-ACLE

CONTRACTING ORGANIZATION: PONTIFICIA UNIVERSIDAD CATOLICA DE CHILE
Santiago, Chile

REPORT DATE: August 2009

TYPE OF REPORT: FINAL

PREPARED FOR: U.S. Army Medical Research and Materiel Command
Fort Detrick, Maryland 21702-5012

DISTRIBUTION STATEMENT:

Approved for public release; distribution unlimited

REPORT DOCUMENTATION PAGE

Form Approved
OMB No. 0704-0188

1. REPORT DATE *(DD-MM-YYYY)*	2. REPORT TYPE	3. DATES COVERED *(From - To)*
10-07-2009	FINAL	11 JUL 2008-10 JUN 2009

4. TITLE AND SUBTITLE

Development of lead compounds as fusion inhibitors for Dengue virus

5a. CONTRACT NUMBER

5b. GRANT NUMBER
W81XWH-08-1-0285

5c. PROGRAM ELEMENT NUMBER

6. AUTHOR(S)
Tomás Pérez-Acle, Ph.D.

E-mail: tperez@bio.puc.cl

5d. PROJECT NUMBER

5e. TASK NUMBER

5f. WORK UNIT NUMBER

7. PERFORMING ORGANIZATION NAME(S) AND ADDRESS(ES)

Pontificia Universidad Católica de Chile
Santiago-Chile

8. PERFORMING ORGANIZATION REPORT NUMBER

9. SPONSORING / MONITORING AGENCY NAME(S) AND ADDRESS(ES)
U.S. Army Medical Research and Materiel Command
Fort Detrick, Maryland 21702-5012

10. SPONSOR/MONITOR'S ACRONYM(S)

11. SPONSOR/MONITOR'S REPORT NUMBER(S)

12. DISTRIBUTION / AVAILABILITY STATEMENT

Approved for Public Release; Distribution Unlimited

13. SUPPLEMENTARY NOTES

14. ABSTRACT
Identification of antiviral agents is critical to the development of therapeutic treatments directed against dengue virus (DENV), for which there is no specific therapy. The structures of the dengue virus class II fusion envelope proteins (E) suggest several features that could be explored as targets for inhibition. This report describes the activities, methods and approaches used for the design and identification of chemical entities targeting the dengue virus fusion process mediated by the E glycoprotein. The compound were designed to target the essential pH dependent conformational changes that occurs in the envelope protein (E protein), by inhibiting the conformational rearrangement that allows the virus-host membrane fusion.

15. SUBJECT TERMS
DENGUE VIRUS, VIRAL FUSION, INHIBITORS, DRUG DESIGN.

16. SECURITY CLASSIFICATION OF:			17. LIMITATION OF ABSTRACT	18. NUMBER OF PAGES	19a. NAME OF RESPONSIBLE PERSON
a. REPORT	b. ABSTRACT	c. THIS PAGE			USAMRMC
U	U	U	UU	61	19b. TELEPHONE NUMBER *(include area code)*

Table of Contents

Introduction

The four serotypes of dengue viruses (DENV1-4) are mosquito-borne transmitted human pathogens and a major burden in many regions of the world by causing diseases that include fatal dengue hemorrhagic fever and the dengue shock syndrome.[1] Recently, dengue viruses were estimated to cause 50−100 million annual human infections worldwide and 22,000 deaths, and dengue fever cases per year is increasing steadily in the United States, where dengue virus has spread to several states and the risk of an outbreak is recognized.[2] To date, no vaccine or therapeutic compound against dengue virus has been approved for clinical use.[3-5] Thus, defense against outbreaks of dengue infection and exposure of US military personnel to the disease might be offered by antiviral agents as a treatment strategy.

The dengue virus envelope glycoprotein as drug target

Recent advances in the structural and molecular biology of dengue virus fusion process have identified the envelope (E) glycoprotein as a novel molecular target with therapeutic potential. Additionally, understanding the dynamics of the flavivirus E protein, suggest three regions within the protein that could be targeted by antivirals: the βOG ligand binding pocket, E-protein rafts in the mature virus and E homotrimers.[6-8] Immature dengue virus at neutral pH is an icosahedral particle with a diameter of ~600 Å and an external coat of trimers of prM:E heterodimers, as shown by cryoelectron microscopy reconstruction.[9] The E protein comprises three domains and is elongated in shape (Figure 1A). Virus entry followed by endosomal acidification induces structural changes, in which E rearranges from 90 homodimers in neutral pH to 60 homotrimers in acidic pH.[10, 11] The interface between domains I and II has been identified as a site for ligand binding; *N*-octyl-β-D-glucoside (βOG) was observed in one crystallographic structure to lie in a buried hydrophobic pocket formed between domains I and II (Figures 1B and 1C).[12] The pocket appears to result from an induced-fit binding because in other structures of the E protein from dengue or tick-borne encephalitis virus a loop connecting the two domains adopts an alternative conformation that closes over and eliminates the pocket. The large-scale structural changes between immature and mature virus, including the differences in domain orientations of dengue E protein, suggest that ligands that binds to this pocket could inhibit a step in the virus lifecycle at which the dengue virus E protein undergoes a structural transition. A similar strategy of targeting a buried pocket in a viral capsid protein was exploited with human rhinovirus, leading to the development of numerous antiviral compounds.[13-16]

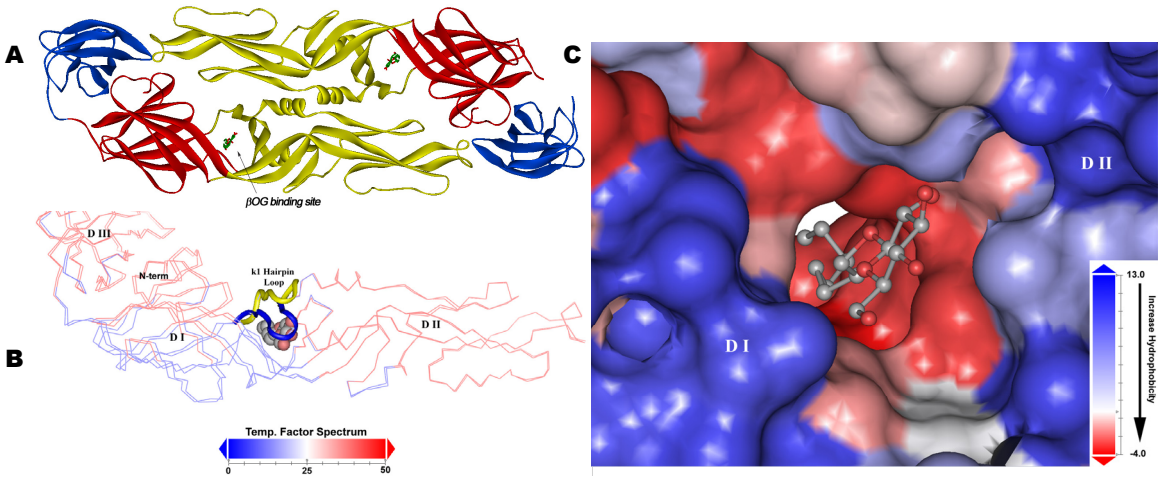

Figure 1 Structural change in DENV2 envelope protein upon βOG binding. A) Secondary structure representation of E2 protein domains I (red), II (yellow), and III (blue). B) Structural alignment of E2 protein monomer in the absence and presence of βOG (pdbIDs 1OAN and 1OKE respectively), with the kl-β hairpin loop colored as follows: prefusion state (yellow), intermediate βOG-E2 complex (blue), secondary structure colored by B-factor from blue (rigid) to red (flexible); C) Snapshot view of the βOG site and groove region with solvent accessible surface with 1.4 Å radius solvent probe, colored red for hydrophobic and blue for hydrophilic.

Body

To develop lead compounds as fusion inhibitors for Dengue virus

The original Statement of Work (SOW) is as follows:

Hypothesis.
Molecules able to mimic all the conformational, electronic and energetic restraints of βOG docked at its crystallographic position against E2 protein, might impair hinge flexibility and presumably interfere with host cell membrane ligand binding, thus disrupting the viral fusion process.

Technical objectives
Task 1. To apply a complex bioinformatics workflow to design a pharmacophore-based library
- a. To perform isosteric replacements and ADME/Tox filtering
- b. To design a fragment based library
- c. To perform isosteric replacements and ADME/Tox filtering
- d. To perform virtual screening methods using the designed compounds libraries

Task 2. To synthesize up to 20 resulting molecules
- a. To separate and characterize the synthesized molecules

Task 3. To perform in vitro biological cell based evaluations for DENV fusion inhibition and toxicity
- a. To obtain at least one bioactive compound**.**

Accomplishments for project

Task 1. To apply a complex bioinformatics workflow to design a pharmacophore-based library.

When the project began we had identified a preliminary pharmacophore hypothesis based on βOG crystallographic position in the DENV E2 protein. Based on this pattern we select preliminary sites for isosteric replacements (Figure 2 A to C)

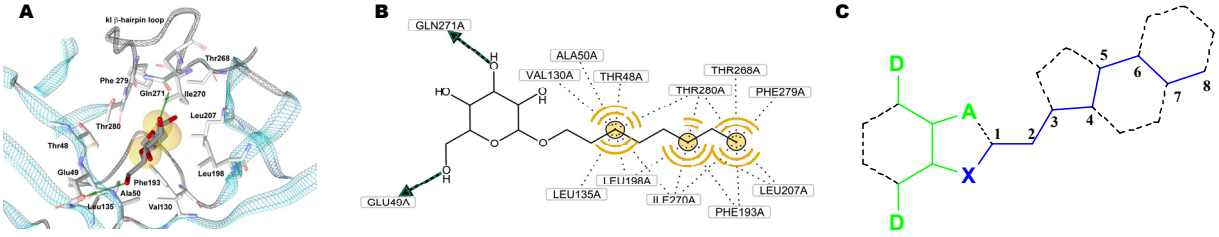

Figure 2 Pharmacophore constrains for βOG-E2 complex. A) βOG binding site in the E2 protein, B) 2D scheme of βOG molecular interactions; C) Schematic representation of basic scaffold designed for isosteric replacement and cyclation.

βOG binding site characterization

On the basis of the available crystal structures of the E2-βOG complex, preliminary target constrains were defined. The βOG binding pocket present in the 1OKE conformer has a dimension of about 10Å in length, 15Å width and 20Å in depth. The pocket is located in the interface of domains I and II (the kl β-hairpin loop, Figure 1B), where several mutations of residues in the interface alter the threshold pH for fusion, and most of them involve side chains in the βOG-binding pocket (Q52, F193, K204, T268, I270, G275I, K277, F279). The pocket is able to accomodate a single βOG molecule, and the polar and hydrophobic contributions for βOG binding at the binding pocket are distributed unsymmetrically, mainly due the presence of hydrophobic residues lining the inner face of the βOG molecule (Figure 1C). In contrast, the outer face of βOG lines with a polar rim that contains polar residues and main-chain peptide bonds that confers this wall an increased polar potential. Thus, it is very advisable to design ligands targeted to

establish favorable contacts with one or more of the most conserved or the most structurally relevant residues lining the binding pocket.

Pharmacophore modeling
The preliminary pharmacophore hypothesis based on the crystal structures of the E2-βOG complex (Figure 1B), consist of:
- 3 hydrophobic features located in the middle on the channel of the binding pocket
- A spatially constrained 18-20 Å long tunnel-shaped pocket
- 3 H-bond donor features and 1 H-bond acceptor feature representing the electrostatics interactions of the hydroxyl groups of the glycoside head in a hydrophilic area at the outer part of the binding site.
- A possibility for H-bond interaction with residues in the inner part of the pocket can be established by some of the potential ligands.

Functional group mapping and fragment placement
A selection of functional groups and commercially available building blocks was selected for fragment-based protein functional group mapping for DENV2 using the Multiple-Copy Simultaneous Search (MCSS) and docking approaches. To establish functional group maps of the protein binding site, the multiple copy simultaneous search (MCSS) methodology[17] was applied in a 15 Å sphere from the center of mass of the βOG molecule. MCSS allows the determination of functional group maps of the protein binding site. MCSS determines energetically favorable position and orientation of functional groups in the binding pocket, by randomly placing the groups in the binding pocket, which are then minimized simultaneously using a force field such that a the forces among individual groups are not considered. Groups are discarded if the interaction energy between them and the protein is above certain threshold. An MCSS run yields a set of pre-docked fragments that can be further investigated to select the most promising ones. The same outcome can be achieved by the use a grid-based method available in several docking software, which is indeed the initial step in some de novo design programs. This placement of chemical groups provides the starting point for the assembly of a complete ligand.
Several polar, charged, aromatic, and aliphatic functional groups have been mapped into the βOG binding pocket. Functional groups of various ring sizes were purposefully chosen to reveal the shape of the binding site; the aromatic groups consist of five-membered, six-membered, and six-membered fused rings, while the aliphatic groups include a nonplanar six-membered ring. Charged groups were chosen to determine the positions in the pocket that could most readily accommodate full or partial charges, which would increase the solubility of a candidate ligand.
The MCSS calculations are summarized in table 1 and examples of group distribution and energy plots are shown in figure 3.

Table 1 Results of Groups Mapped into the DENV E2 βOG binding site

Group	Chemical label	ΔH/2 (kcal/mol)	N° of copies	Minima with interaction energy<0	Range of minima interaction energies (E_M)*	Minima with interaction energy<ΔH/2
BENZ	Hydrophobic	-3,5	200	89	-18.19; -0.87	84
ACET	Acceptor	-46,5	200	105	-117.56; -0.47	16
CHEX	Aliphatic		200	148	-9.07; -0.26	
2BTN	Neutral		200	198	-10.45; -4.74	
ACAM	Acceptor, Donor	-9,6	200	198	-50.3; -3.55	151
MAMM	Donor	-37,5	200	95	-131.04; -0.24	61
OXAZ	Acceptor, Donor		200	198	-30.72; -9.88	
TRPR	Aromatic		200	198	-22.89; -9.09	
WATR	Dual	-5,0	200	189	-46.8; -0.65	173
HISR	Dual		200	198	-42.12; -10.51	

**All energies are in kilocalories per mole. $E_M = E_I - E_0$, where E_I is the interaction energy of the group with the protein including the internal energy terms of the group and E_0 is the vacuum reference energy for the group. ΔH/2 corresponds to half of the solvation energy for the corresponding group.*

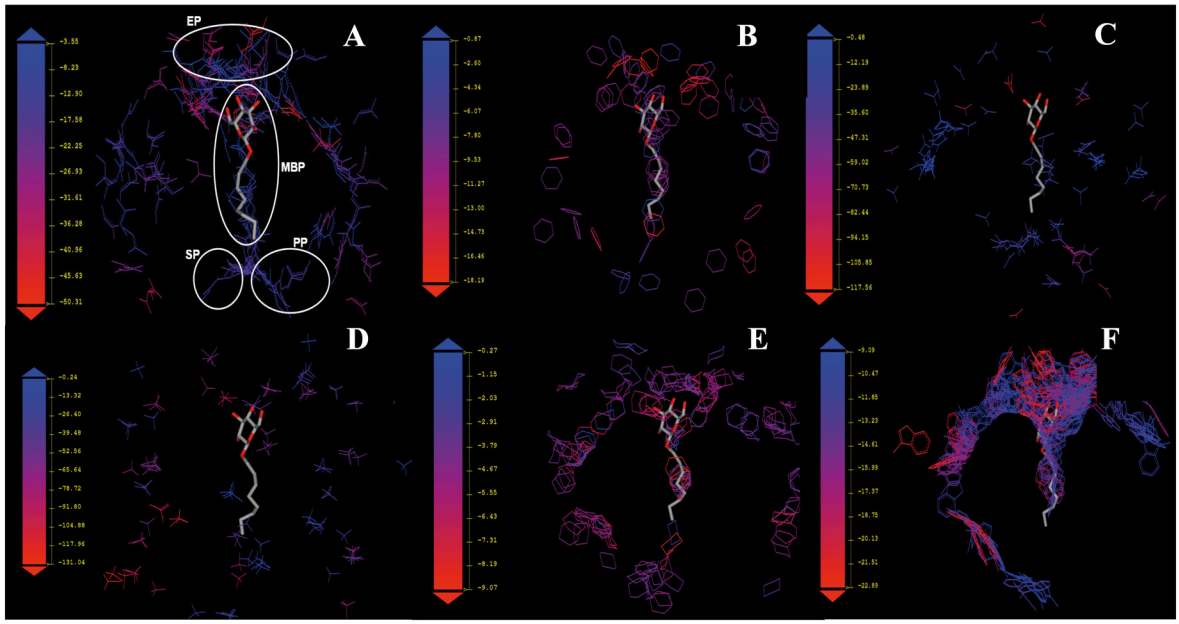

Figure 3. Functional group maps of DENVE2 βOG binding site A) ACAM minima with energy <9.6 kcal/mol. B) BENZ minima with energy <5.1 kcal/mol. C) ACET minima with energy <46.5 kcal/mol. E) MAMM minima with energy <37.5 kcal/mol. All other functional group maps are of minima with energy <0. F) CHEX minima. G) TRPR minima. (Definitions of the groups are in Table 1).

The minima for many of the groups are shown in Figure 3. The βOG molecule, which was removed for the calculations, is shown in each figure so that the minima for the different functional groups can be compared. Many of the functional groups have minima in the main binding pocket (MBP in Fig. 3A), in a newly identified polar and side pockets (PP and SP in Fig. 3A), and at the entrance to the pocket (EP in Fig. 3A). There are also a few positions at the edge of the binding site sphere where most functional groups have minima; these are small pockets on the surface of the protein that are uninteresting in terms of drug design. After mapping the different functional groups in the binding site, the best minima from each obvious cluster can be connected to form potential drug molecules and functional groups maps can be compared with our preliminary pharmacophore hypothesis.

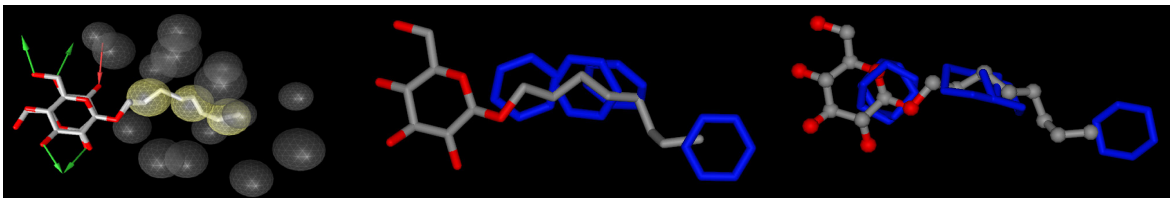

Figure 4 From left to right. Comparison of the location of preliminary pharmacophore hypothesis with MCCS selected solution for BENZ and CHEX probes within the binding site.

As can been seen from figure 4, the results of the MCSS calculations selected minima position supports our preliminary pharmacophore hypothesis and suggest various ligand design strategies. Ligands could be designed for the main binding site, the side pocket, the polar pocket, or the main binding site plus the polar pocket. For the main binding site, the ligands could be comprised primarily of aromatic or non aromatic rings. We have concentrated on designing new ligands for the main binding pocket that include aromatic functional groups because the six member aromatic and aliphatic ring minima form obvious clusters in the main binding pocket, and for the polar pocket, where most of the polar groups form clusters as well.

Fragment placing using molecular docking simulations

Similar results were obtained when a fragment libraries designed by: a) isosteric replacements of the βOG scaffold over the preliminary pharmacophore hypothesis, and b) a heterocycle fragment library, were docked in the βOG binding site using a grid-based approach. Fragments were docked into a 15Å sphere surrounding the βOG binding site. Further re-ranking and solution selection were used to map potential interactions sites and to probe the binding site volume constrains. As can be seen in figure 5, an L-shaped distribution of the solutions through the main binding pocket with a wide variety of heterocyclic moieties and the polar pocket with small acyclic groups and 5-6 member rings with H-bond donors or acceptors (*see Addendum 1 for structures and their binding energies*).

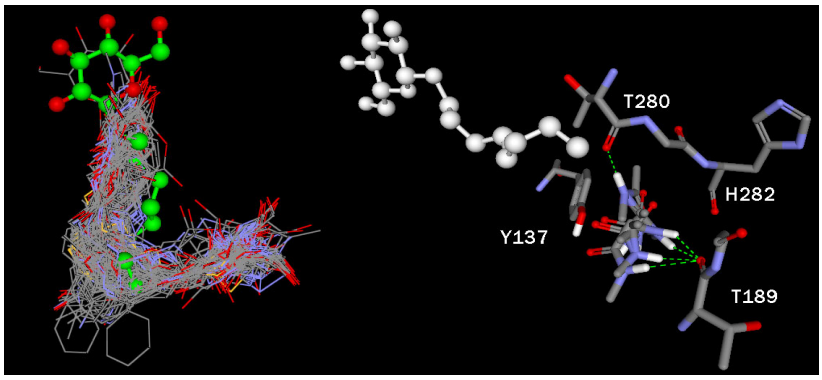

A **B**

Figure 5 A) MVD docking results. B) Snapshot of the detected polar pocket residues and potential interaction with ACAM probes.

The polar pocket consists of several residues that can establish favorable ionic interactions with ligands. For the ACAM probe, the main chain CO group of Thr189, His282, Thr280 and the phenol side chain of Tyr137, could be targeted for this purpose. The results indicate that this combinatorial method has considerable potential for designing structure-based *de novo* ligands by computational methods.

Fragment linking and assembly

As stated before, the MCSS and docking approaches output is a set consisting of one minimum from each cluster. To link the clusters, the coordinates of the nearest bound βOG carbon position or the location of carbon based probes were used. Then the connectivity of the links was optimized, while the functional groups were held fixed in their minimum energy positions. In this way, a structure that has the combination of links with the lowest energy is constructed and further optimized. Some examples rising from the MCSS and MVD results are showed in figure 6. For the MCSS example (A), the βOG molecule was extended into the polar pocket using a methyl minima near the their carbon atom of the alkyl chain in βOG, a piperidine minima and finally an 1,3-oxazole moiety was added, resulting ligands position and potential interactions are also shown. For comparative purposes, in the MVD example (B) we also select a piperidine moiety but were linked at position 2 in the alkyl chain and then a dimethylisoxazole moiety was added, but other βOG head conformer was used instead.

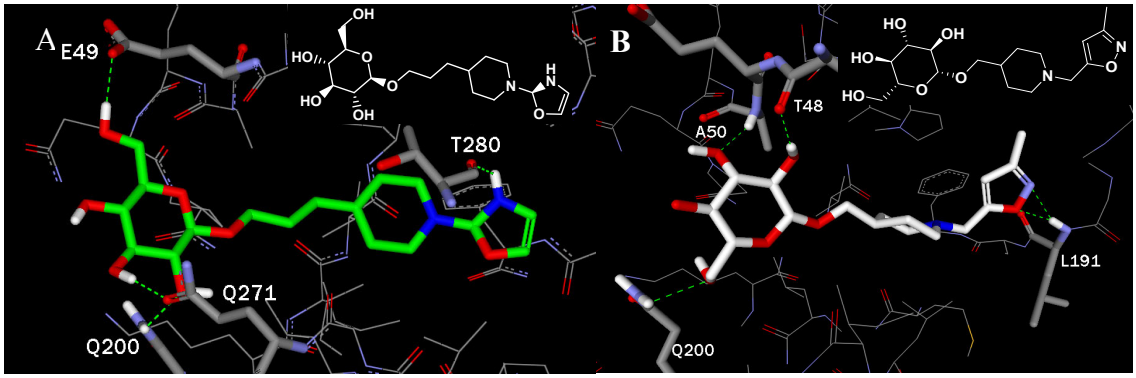

Figure 6. Examples of A) MCSS based group link and assembly, and B) MVD fragment assembly. Some residues are omitted for clarity.

These are examples of ligands designed to target the MBP and the MBP plus the PP respectively. In both examples the glycoside main electrostatic interactions are conserved while new interactions can be formed with the backbone of residues lining the MBP or the PP. The results suggest that candidate drugs designed using this approach could bind at least as well as βOG or the fragments used in ligand assembly, assuming that they are able to enter the pocket in a similar manner and have been connected with minima having favorable interaction energies with the target protein.

Secondary Pharmacophore Hypothesis Generation

The MCSS and MVD results also led us to propose a secondary pharmacophore hypothesis. As can be seen in figure 7A, a secondary pharmacophore hypothesis can be obtained from the placement of different fragments or assembled ligands into de βOG binding site.

For the latter example of the MVD fragment approach the pharmacophore hypothesis consist of:

- 2 Hydrophobic features located in the middle on the channel of the binding pocket and at the end of the polar pocket
- 13 exclusion spheres
- 1 aromatic feature in the center of the polar pocket
- 1 H-bond donor features and 2 H-bond acceptor feature representing the electrostatics interactions of the hydroxyl groups of the glycoside head in a hydrophilic area at the outer part of the binding site and the electrostatic interaction in the polar pocket.

Furthermore, a shared pharmacophore containing the features and constrains of our preliminary and second generation pharmacophore is proposed (Figure 7B). In this way, as in the fragment approaches, these different pattern-based pharmacophores were exploited for virtual screening of compounds databases in search for ligands targeting the MBP or the MBP/PP. The main advantage of a 3D database pharmacophore searching over *de novo* design is that the former one is capable of identifying molecules which can be obtained from corporate compound libraries or can be synthesized using a well-established protocol.

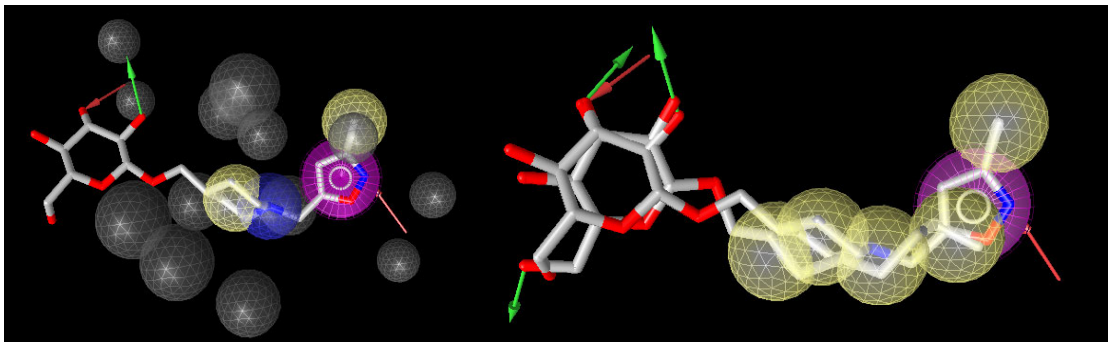

A **B**

Figure 7 A) Secondary MVD based pharmacophore hypothesis and, B) Shared feature pharmacophore targeting the MBP and the PP protein functional sites.

Pharmacophore focused library generation.

Fragment assembled ligands used to create the secondary pharmacophore hypothesis suggest compounds with the general structure consisting in a polar glycosyl head, a linker region and a small H-bond acceptor/donor aromatic or aliphatic group (figure 7B). Entrance into this hydrophobic pocket through a narrow pore on the capsid surface requires a certain amount of flexibility of the compounds. However, MVD results for large ring systems are allowed because of steric restrictions of the tunnel-shaped binding site don't exclude high volume heterocyclic moieties. Studies on the characteristic structural framework of our pharmacophore hypothesis guided parameter setting and the following generation process within the ilib diverse software.[18]

For exhaustive representation of secondary pharmacophore characteristics, the ordered group modus is selected and a number of 5 flasks were defined for the library generation process. Figure 8 shows the important sections for the MVD example compound molecule and helps to explain the design of the focused libraries based on our secondary pharmacophore hypothesis.

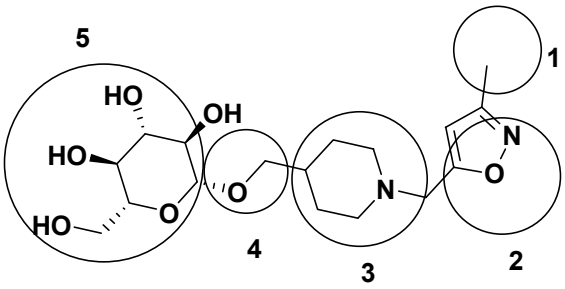

Figure 8 Division of MVD example compound into five building blocks used for flask definition in ilib diverse.

Flask 1: This substituent filling the innermost part of the binding pocket may be composed of a small rather lipophilic group. Our fragment selection includes Methane and Ethane contained in the Aliphatics fragment set, Fluoride from the Halogen, and Trifluoromethyl from the Fx groups. The methyl residue was observed frequently in the MVD resulting compounds at this position; the Methane fragment was given a weight of 100%.Trifluoromethyl, was provided with a weight of 50%, whereas the other weight values were set to 20%.

Flask 2: This moiety consists of aromatic or semi-aromatic 5 or 6-membered heterocyclic rings. Rings at this position present a well conserved pattern in the MVD solutions. We include therefore several 5-membered rings from the heterocycles fragment set into this flask: 1,2,4-Triazole, 1,3,4-Thiadiazole, 1,3-Thiazole, Furane, Isothiazole, Oxazole, Pyrazole, Pyrrole, Tetrazole, and Thiophene. Commonly observed docking solutions at this position is the Oxazole, which is therefore given a weight of 100%. Reactivity settings of 10 and 5 for the carbons in position 2 and 4 respectively were used to guide the generation process into the desired direction. A weight of 100% is adequate for another favourable heterocycle. Reactivity values for the other fragments remain at their default values, and their weights were set to 20%.

Flask 3: For this methyl-, chloride-, or non-substituted benzene moiety, a set of predominantly newly created fragments were selected: Benzene, Chlorobenzene, Dichlorobenzene, Chloromethylbenzene, Toluene, Dimethylbenzene, Fluorobenzene, Difluorobenzene, and Fluoromethylbenzene. Another bulky aliphatic and aromatic heterocycles such as Piperazine, Piperidine, Pyridine were included. Reactivity values for the benzene ring atoms at position 2 and 4, respectively, were increased. Other possible starting points for substitution were prohibited by the setting of negative reactivity values.

Flask 4: An aliphatic chain of 2 to 5 atoms of length creates a linkage to the glycoside ring situated rather at the pocket entrance region. Therefore C2 to C5 saturated, linear alcohols were selected. Reactivity of the oxygen atom as increased to 10 in order to enforce the by default prevented substitution and consequently resulting ether generation at this position. The terminal oxygen atom of the chain, the desired target for the second substitution process, was set to a reactivity value of 3, whereas other atoms of the chain were protected from reaction by negative reactivity values.

Flask 5: The last building block filling the entrance region of the pocket consists of a glycoside ring, which is known from X-ray structure information to enable favorable polar interactions with the outer part of the binding site. Maximum reactivity was defined at position 5 of this ring system. Nevertheless, since the binding site also offers room for larger-sized residues, other fragment selected from similarity searches were included.

Filter Settings

Application of the 'Lipinski rule of five' filter ensures high drug-likeness and oral bioavailability of the generated compounds. Stereochemistry setting is defined as by default (assign mixed stereo chemistry), but no chemical modification was desired because of the high specificity of the fragment definition.

This generation process results in a drug-like library of compounds that share the same shape and the same functions as the secondary pharmacophore hypothesis. They are therefore promising candidates for virtual screening, synthesis and biological testing. Out of the generation process, more than 80% of the structures did not match the filter requirements, especially the desired estimated log P, and were therefore rejected.

ADME constrains

The primary goal of the application of *in silico* ADME profiling during the hit identification stage was to identify compounds or series with the least acceptable drug-like properties to eliminate them from consideration. The risks of this approach are the potential for false positives and false negatives. False positives are easier to resolve because they will be subjected to other tests further into the process that

will eliminate them. False negatives are potentially more contentious because of the risk of missing some potential. However, owing to the large numbers of compounds involved (up to millions), the law of probability ensures that many compounds with potentially good characteristics will make it through. Another goal of ADME application here is to identify potential weaknesses and liabilities in the designed series to highlight the issues that will form the focus of improvement/ optimization efforts.

Clinical aspects of dengue virus infection and pathogenesis were also considered into our design hypothesis. Briefly, after an infected mosquito has bitten a person, the virus replicates in regional lymph nodes and is disseminated through the lymphatic system and blood to other tissues, and replication in the reticuloendothelial system and skin results in viremia. The incubation period ranges from 3 to 14 days, but it is usually 4 to 7 days.[14] Infection with dengue virus of any of the four serotypes causes a spectrum of illness, ranging from no symptoms or mild fever to severe and fatal hemorrhage, depending largely on the patient's age and immunologic condition.[19, 20] Another important issue is related to the cellular localization where the E2 protein adopts its fusogenic conformation, that is, inside the endosome.[21]
Thus, preliminary ADME filtering was consider to achieve these objectives and to establish some basic limits to the physicochemical properties of potential ligands, while maintaining potency.

Lipophilicity. Poor biopharmaceutical properties in particular, poor aqueous solubility and slow dissolution rate, can lead to poor oral absorption and hence low oral bioavailability. In general, poor solubility is related to high lipophilicity, whereas hydrophilic compounds generally show poor permeability and hence low absorption. Therefore, the measurement of solubility and lipophilicity, as well as ionization constants affecting these two properties has been integrated in our drug discovery program. Lipophilicity is the key physicochemical parameter linking membrane permeability, and hence drug absorption and distribution with the route of clearance (metabolic or renal). Measuring the lipophilicity of a compound is readily amenable to automation. For our purpose, we establish the -5 to 5 logP units as preliminary filter when designing our series, subsequent stringent criteria was applied in the selected hits.

Solubility. The first step in the drug absorption process is the disintegration of the tablet or capsule, followed by the dissolution of the active drug. Obviously, low solubility is detrimental to good and complete oral absorption, and so the early measurement of this property is of great importance. Reflecting this need, we also have include this filter, because, ideally, only soluble compounds would be synthesized, the compounds must have a logSw > -4 for electrolytes and logSw > -3 for non-electrolytes.

pKa. As ionization can also affect the solubility, pH dependent partition coefficient (log D), permeability and absorption of a compound, batch calculations procedures can be used for the rapid measurement of pKa values of sparingly soluble compounds. Considering the pH range where the E2 protein suffers its conformational changes, the preliminary limits for pKa values were established to be < 6 for weak bases and > 6 for weak acids.

Hydrogen bonding. The hydrogen-bonding capacity of a drug solute is an important determinant of permeability. In order to cross a membrane, a drug molecule needs to break hydrogen bonds with its aqueous environment. The more potential hydrogen bonds a molecule can make, the more energy this bond breaking costs, and so high hydrogen-bonding potential is an unfavorable property that is often related to low permeability and absorption. To characterize the hydrogen bond capacity of the designed libraries, the Abraham's solvation parameters were also included.[22]

Bioavailability. Bioavailability depends on a superposition of two processes: absorption and liver first-pass metabolism. Absorption in turn depends on the solubility and permeability of the compound, as well as interactions with transporters and metabolizing enzymes in the gut wall. Important properties for determining permeability seem to be the size of the molecule, as well as its capacity to make hydrogen bonds, its overall lipophilicity and possibly its shape and flexibility. First pass susceptibility to metabolic transformations catalyzed by enzymes in liver and intestine has been established in the range of 50-70% for discarding potential compounds.

Absorption. For a compound crossing a membrane by purely passive diffusion, a reasonable permeability estimate can be made using single molecular properties, such as logD or hydrogen-bonding capacity. However, besides the purely physicochemical component contributing to membrane transport, many compounds are affected by biological events, including the influence of transporters and metabolism. Many drugs seem to be substrates for transporter proteins, which can either promote or

hinder permeability. In particular, the combined role of cytochrome P450 3A4 (CYP3A4) and P-glycoprotein (P-gp) in the gut as a barrier to drug absorption has been well studied. We introduce in our ADME filtering protocol the estimation of the probability of suffering extensive 1st pass metabolism and the probability of the compound to be transported by P-glycoprotein (P-gp) as substrates and/or inhibitors. Substrates are compounds that are transported (effluxed) by P-gp. Inhibitors are compounds that block P-gp transport of the standard substrates (calcein-AM and others). The classification models, used P-gp substrate and inhibitor specificity rules, based on ionization, molecular size and biological class of compounds (analogs of peptides, alkaloids, anthracyclines, etc.). We therefore have included the prediction of the effect of a compound's physicochemical properties: LogP, pKa(acid), pKa(base) on the upper limit of its intestinal passive absorption via both transcellular and paracellular routes, its human jejunum and Caco-2 permeabilities, and its absorption rate.

Blood–brain barrier penetration. Drugs that act in the CNS need to cross the blood–brain barrier (BBB) to reach their molecular target. This is important considering that flavivirus encephalitis and dengue fever are characterized by membrane permeability increase that allows virions to reach the brain.[23, 24] By contrast, for drugs with a peripheral target, little or no BBB penetration might be required in order to avoid CNS side effects. Recommendations regarding the molecular parameters that contribute to the ability of molecules to cross the BBB have been made to aid BBB-penetration predictions; and for designed purposes, molecules with a molecular mass of <350 Da or with PSA <100 $Å^2$ are more likely to penetrate the BBB.[25]

Transporters. Transport proteins are found in most organs involved in the uptake and elimination of endogenous compounds and xenobiotics, including drugs. As mentioned above, a better understanding of the role of transporters in oral absorption and uptake in the brain and liver is of particular interest. We have included the PepT1 (oligopeptide transporter) and ASBT (bile acid transporter) substrate prediction.

Plasma-protein binding*.* It is generally assumed that only free drug can cross membranes and bind to the intended molecular target, and it is therefore important to estimate the fraction of drug bound to plasma proteins. Drugs can bind to a variety of particles in the blood, including red blood cells, leukocytes and platelets, in addition to proteins such as albumin (particularly acidic drugs), α_1-acid glycoproteins (basic drugs), lipoproteins (neutral and basic drugs), erythrocytes and α, β, γ-globulins. Considering that one of the main physiological compartments where the virus exists in humans, we have included the estimation of the compounds binding to plasma proteins in general and specifically to albumin.

Volume of distribution. The volume of distribution, together with the clearance rate, determines the half-life of a drug and therefore its dose regimen, and so the early prediction of both properties would be of great benefit. We have only included for this phase the estimation of the volume of distribution.

Very importantly, the βOG molecule has never been reported to inhibit the fusion process and whether βOG-based designed ligands could become useful drugs, even if their binding is confirmed, involves many other factors, such as drug delivery, toxicity, and resistance.

An example of comparative ADME profiling is illustrated in the following two examples and compared with βOG profile.

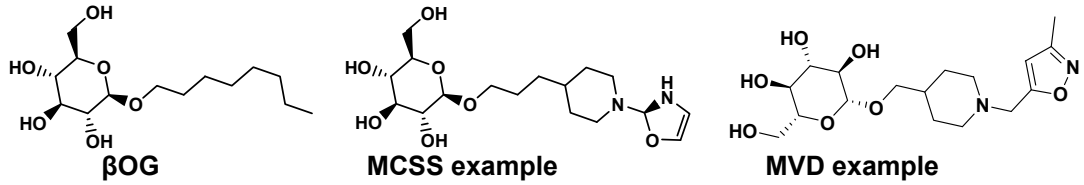

Figure 9 Chemical structures of example compounds

Addition of polar moieties to the βOG alkyl chain produces an increase in solubility and bioavailability, due the effect of ionizable groups present, mainly in the MVD example where the piperidine N atom can be ionized. All generated ligand in the library were stable at acidic conditions, and were favored to distribute in the plasma. Passive transport across GI diminishes and contribution of the paracellular route becomes

more important. None of the ligands were estimated to bind P-gp or to be actively transported. Blood-brain barrier penetration is possible but is impaired by the low logP and topological surface area.
Finally, a virtual library of ~500.000 drug-like compounds was obtained.

Virtual screening

Using the current structural information on dengue E2 protein, several groups have conducted virtual screening (VS) experiments to identify potential hits directed towards the βOG binding site (Figure 10 A, B and D)[26, 27] and alternative cavities (Figure 10 C)[28], or have used the E2-βOG complex as starting point but the identified compounds were evaluated in YFV inhibition assays, but the bis-amidinohydrazone derivative probed to bind the dengue E2 βOG binding site by saturation transfer NMR experiments (Figure 10 E).[29, 30]

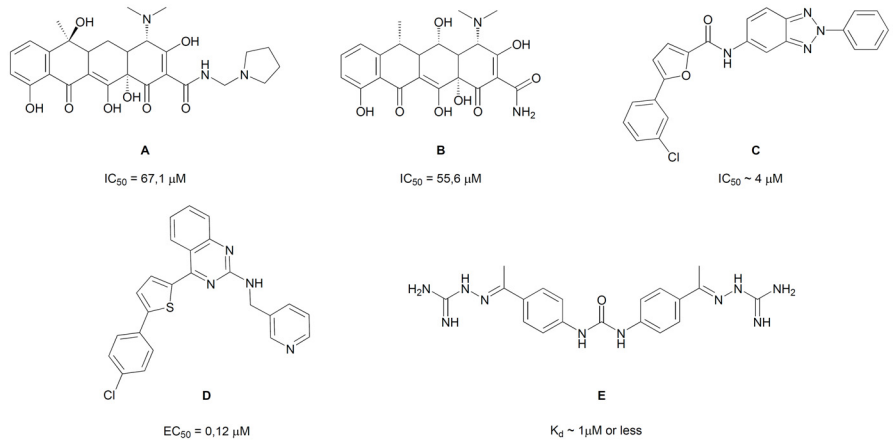

Figure 10 Reported dengue virus 2 fusion inhibitors.

Before attempt to perform our own virtual screening experiments with large libraries of compounds, we first assessed the reliability of the Autodock 4 (AD4) docking method applied to the targeted site of dengue E2 protein. The reliability of the designed protocol was demonstrated by docking βOG and comparing the results with the known structure of the crystallographic complex. The results for the best ranked docked pose (defined by ligand conformation and docked position) in the best cluster scored using the AD4 function was selected for comparison. The root-mean-square deviation (RMSD) of βOG heavy atoms between the best docked pose and the crystallographic coordinates after superposition of E protein was less than 1.5 Å (Figure 11A). The results are evidence that AD4 can accurately reproduce the known structure of the E protein- βOG complex.

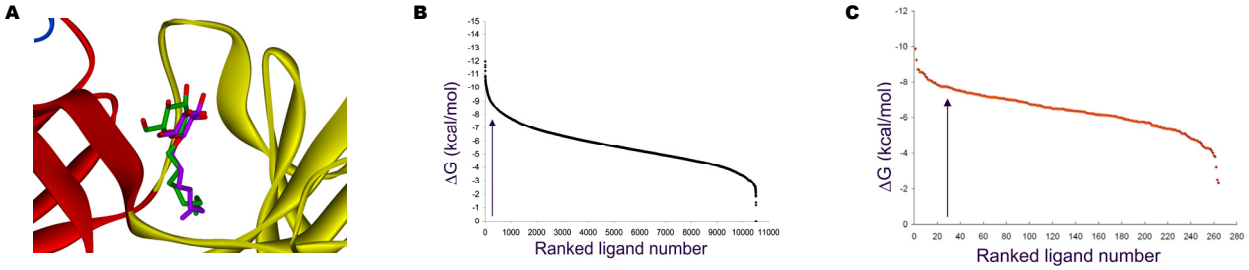

Figure 11 A) The superposition of AD4 best docked pose (cyan carbons) (stick) with the crystal structure of βOG (green carbons) bound to E2 protein (ribbon) in the pocket between domain 1 (red) and domain 2 (yellow). RMSD between the docked and experimental position of βOG was 1.22 Å. B) Plots for stage 1 (AD4 scoring function) and B) stage 2 (Ludi scoring function). In both cases, a similar to a Gaussian profile with a rapid initial drop over a small number of the most favorable compounds, followed by more slowly decreasing scores for a substantially larger number of compounds and a sharp fall off as the scores approach zero in value. The arrow indicates the cutoff points for selection of each corresponding subset.

After validation of the docking protocol, we performed a preliminary VS procedure to identify small-molecule ligands with potential to bind the βOG pocket in dengue E protein. A three-stage protocol (Scheme 1) was used to screen ligands to bind the βOG pocket of E2 protein. The compounds in the library have diverse structures. When this study was initiated, the compounds were available from NCI for biological evaluation.

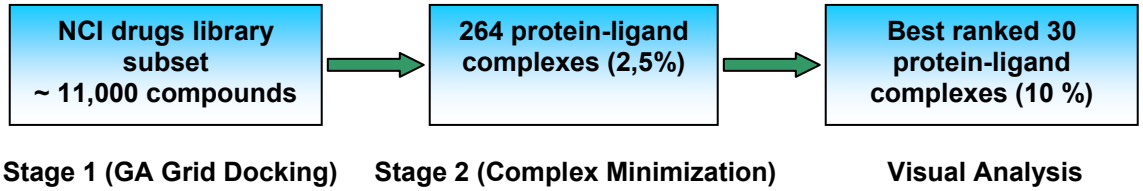

Scheme 1 Virtual screening protocol for identification of potential DENV E2 binding compunds from the NCI diversity set.

The protocol consists of a primary stage that performs a grid-based docking with the following parameters: a 62x40x40 grid size was used with a 0.375 point/Å resolution, 2,500,000 energetic evaluations, 100 runs of the genetic algorithm (GA), an initial population size of 200 individuals per ligand, the rest of the parameters for the docking input file was set as default. The best docked solution (lower binding energy) as ranked by the AD4 force-field based scoring function was selected. A selection criterion of an estimated IC_{50}< 0.5 μM was used to select the best ranked 2.5% of ligands. The ranked AD4 scores for the library following rigid docking (stage 1) are shown in Figure 14A, where lower ranked compounds are plotted by increasing value along the abscissa. Each of the selected 264 protein-ligand complexes were further submitted to a molecular mechanics energy minimization using the CHARMm force-field allowing the flexibility for both the ligands and a subset of protein residues surrounding 15Å from the βOG binding site. Final energy evaluation and ranking of the solutions was performed using the Ludi 2 empirical scoring function (*see Addendum 2*). The obtained minimized protein-ligand complexes were the visually analyzed to rationalize the binding modes and validate original design criteria. Figure 12 show the structure and binding mode of the top 3 scoring compounds after minimization.

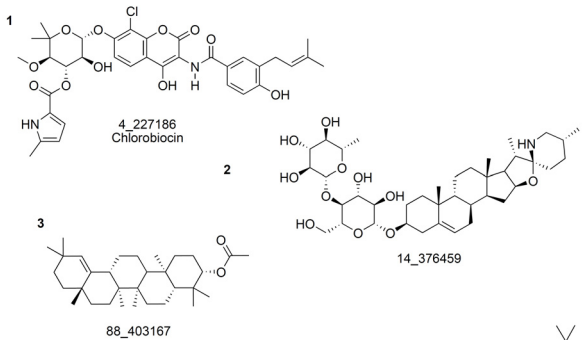

Index2	Ligand	Index	ΔG Ludi2
1	4_227186	4	-9,87
2	14_376459	14	-9,25
3	88_403167	88	-8,71
4	262_374897	262	-8,70
5	65_178260	65	-8,56
6	66_179187	66	-8,56
7	75_111341	75	-8,55
8	1_134905	1	-8,50
9	37_104793	37	-8,44
10	125_82149	125	-8,32
11	81_60677	81	-8,25
12	30_26643	30	-8.14

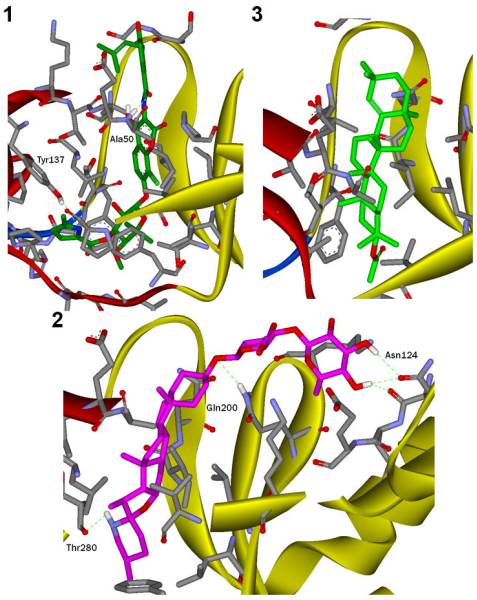

Figure 12 Selected top scoring compounds from the NCI drug library. Ligands numbers denote ranking previous to minimization and NSC numbers. Estimated binding energies are also shown.

Additional work performed, but not included as milestones were the development of comparative models for the other DENV serotypes (1, 3 and 4) glycoprotein's in complex with βOG using Modeller. Figure 13 shows the sequence alignment of DENV envelope proteins.

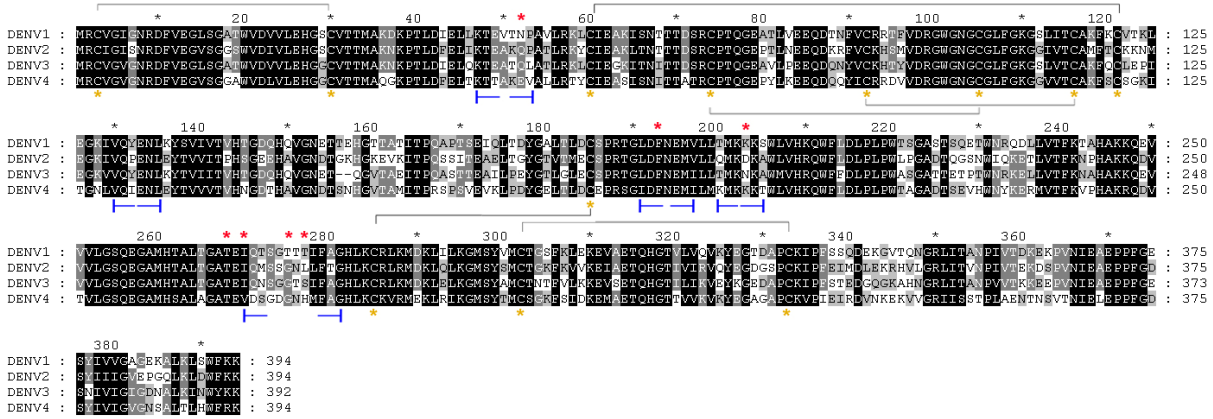

Figure 13 DENV envelope proteins sequence alignment. Brown asterisks and gray lines denotes residues involved in disulfide bridges, red asterisks denotes residues for which mutants changes the pH threshold for activation. Blue bars denote residues lining the βOG binding site in E2.

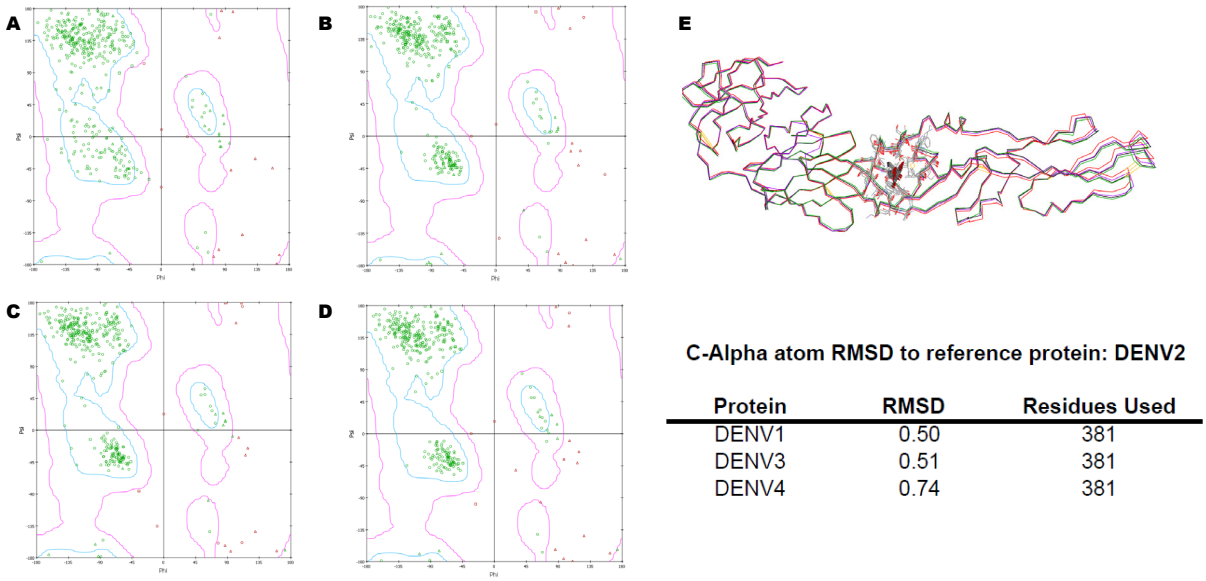

C-Alpha atom RMSD to reference protein: DENV2

Protein	RMSD	Residues Used
DENV1	0.50	381
DENV3	0.51	381
DENV4	0.74	381

Figure 14 Comparative modeling of DENV envelope proteins. Dengue virus envelope protein were modeled with βOG, with less than 1 A, as expected by the high degree of sequence identity among E proteins.

Dengue virus homology obtained E protein models coordinates (DENV1, 3 and 4) plus E2 were used to screen a large library composed of our in-house developed and a set of drug-like compounds compiled from several vendors (Scheme 2). The protocol involves a primary shape-based screening based on the primary pharmacophore definition, which filtered the top 10% according to shape complementarities. The filtered compounds were subjected to a genetic algorithm-based virtual screening campaign, which filtered the top 0,1% according to the estimated binding energy, using the parameter that allows the reproduction of the observed crystallographic position of βOG in DENV2 (Figure 11A). The filtered drug-proteins complexes followed a molecular mechanics energy minimization protocol as a secondary filter, to considering protein flexibility within 15 Å of the βOG binding site. A final consensus scoring scheme selects the finally reported list of compounds. For this task an automated docking web service-based

bioinformatics workflow was developed. This tool allows for automatic preparation of ligand and proteins, virtual screening and post processing and annotation of coordinates and binding energy for each ligand.

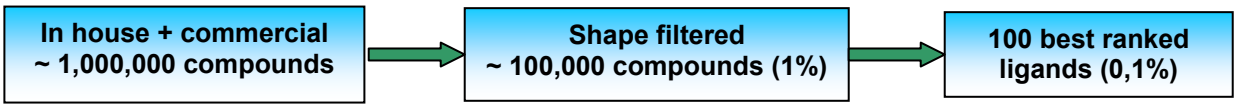

Scheme 2 Parallel virtual screening protocol for the identification of potential DENV E1-4 binding compounds from the developed library and commercial compounds databases subsets.

These additional tasks allow us identify a series of potential broad-spectrum agents by performing comparative virtual screening of our developed library in searching for broad spectrum agents, using our developed virtual screening platform. Figure 15 show the structure and binding mode of a subset of the top scoring compounds after minimization.

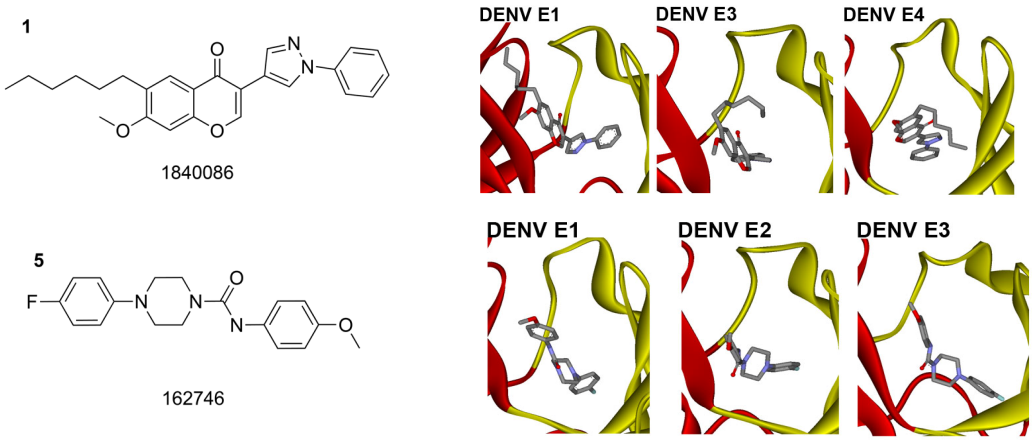

Figure 15 Selected top scoring compounds from the parallel virtual screening of compounds libraries on DENV E 1-4 proteins. Estimated binding energies were averaged to identify potential broad spectrum agents. Binding modes obtained for E proteins is depicted.

From the top 100 best scored ligands we select 62 compounds for biological assays. The ligands were assessed for commercial availability and were obtained from Chembridge, ChemDiv, Enamine, Asinex and Interbioscreen collections.

Reportable outcomes:

- A set of the top 30 compounds from the list of 264 compounds selected from the NCI dataset with potential Dengue virus type 2 fusion inhibitor, stated as a IC_{50} of 5 μM or less, were requested to NCI to perform plaque reduction assay for DENV1 for fusion inhibitor activity.
- A list of drug-like commercially available compounds with potential broad-spectrum activity against DENV 1-4 strains.
- A set of DENV envelope protein model coordinates that can be used for virtual screening or other molecular modeling purposes (Ex. Comparative molecular dynamics).
- Functional group maps for DENV 1-4 βOG binding sites coordinates useful for de novo ligand design
- Second generation and a shared-feature pharmacophore hypothesis for the βOG binding site in DENV envelope proteins.
- 3 Abstracts in scientific meeting (1 poster presentations, 2 oral communication).
- 1 Manuscript in preparation

Task 2. To synthesize up to 20 resulting molecules

Task 2 was replaced for acquisition of commercially available molecules in the meantime. Although we have previously proposed the synthesis and characterization routes for a few molecules (20), We have considered the goals of the project and remaining time to prefer to perform a preliminary screening for cytotoxicity and biological evaluation and follow-up on chemical series with antiviral activity for lead optimization by inclusion of fragments to the binding mode of bioactive scaffolds according to second generation pharmacophore feature definitions. For this purpose a set of 62 small molecules from the library was acquired from several chemical vendors and are currently been assayed for cytotoxicity and DENV1 fusion inhibitory bioactivity using cell-based methods.

Reportable outcomes:

- A set of 62 pure and analyzed (IR, 1H-NMR, 13C NMR, physical constants and elementary analysis) molecules available for biological assays (*see Addendum 3*)

Task 3. To perform in vitro biological cell based evaluations for DENV fusion inhibition and toxicity

Viruses are obligate intracellular parasites. Thus, inhibitors of virus replication must do so without toxic effects on the cells, tissues, and organs of the host. This is the concept of 'selective activity' against viruses. For dengue viruses which form plaques in a cell monolayer, reduction in plaque formation has long been regarded as the 'gold standard' assay. Antiviral activity is usually defined as the concentration of the inhibitor which reduces viral plaques by 50% (50% effective concentration; EC_{50}). Alternatively, the reduction in the yield of infectious virus can give useful information by using different multiplicities of infection (MOI); in such assays, the concentration of inhibitor to reduce replication by 99% (EC99) is usually reported. For some viruses, for example, HBV, reduced production of a measurable virus product (e.g., nucleic acid or protein) is the only way to assess viral replication. For inhibition of a viral enzyme, the 50% inhibitory concentration (IC50) is commonly reported. Irrespective of the antiviral assay, it is necessary to assess cellular toxicity of the test compound. This is essential to eliminate the possibility that the lack of virus replication is due to the destruction of the cells. However, the ratio of the concentration to inhibit the replication of the virus to the concentration to destroy non dividing cells in a monolayer is not an indication of selective activity. To determine selective activity, it is essential to compare like with like, replicating virus with replicating cells. To test for an effect on replicating cells, it is necessary to aim for a tenfold increase (just over three doublings) so that at the 50% cytotoxic concentration (CC50), at least one doubling has occurred and the second round of replication has started. The ratio of 50% viral inhibitory concentration to 50% cytotoxic concentration is defined as the selective index (SI).

We are in the process of evaluating the cytotoxicity and bioactivity of the selected compounds on cell-based assays for DENV1 infection. Virus source corresponds to plasma of acute-phase patient infected with DENV1 strain available at the Laboratory of Molecular Virology at PUC. The toxicity for cells of each selected compound is being established using the quantitative colorimetric MTS method using commercial CellTiter 96® AQueous One Solution Cell Proliferation Assay (Promega Corp., Madison, WI) and will be evaluated in its ability to reduce DENV1 infection of Vero cells using plaque reduction protocol. Plaque titrations will be performed under agarose overlay in Vero cell monolayers and viral infection will be monitored by RT-PCR.

Reportable outcomes:

- A method for concentrating DENV1 from patient plasma.
- A method for DENV1 fusion inhibitor screening.

Key Research Accomplishments

- Development of a pharmacophore based virtual compound library, filtered under stringent ADME/Tox parameters.
- Development of a web service-based bioinformatics workflow for automated docking procedures.
- Development of comparative models of envelope proteins for Dengue virus strains 1, 3 and 4.
- Identification of functional group maps for dengue virus envelope proteins.
- Identification of 264 molecules with potential fusion inhibitory activity against Dengue Virus 2 strain, available for request from NCI.
- Identification of 62 diverse chemical entities with potential broad spectrum fusion inhibitory activity against Dengue virus strains 1-4.
- Development of a method for concentrating DENV1 from patient plasma.
- Development of a method of screening for DENV1 fusion inhibitors.
- Determination of the pharmaceutical profile of the identified compounds.
- Evaluation of the cytotoxic character of each compound in diverse cell lines

Reportable outcomes:

- A set of the top 30 compounds from the list of 264 compounds selected from the NCI dataset with potential Dengue virus type 2 fusion inhibitor, stated as a IC_{50} of 5 μM or less, were requested to NCI to perform plaque reduction assay for DENV1 for fusion inhibitor activity.
- A list of drug-like commercially available compounds with potential broad-spectrum activity against DENV 1-4 strains.
- A set of DENV envelope protein model coordinates that can be used for virtual screening or other molecular modeling purposes (Ex. Comparative molecular dynamics).
- Functional group maps for DENV 1-4 βOG binding sites coordinates useful for de novo ligand design
- Second generation and a shared-feature pharmacophore hypothesis for the βOG binding site in DENV envelope proteins.
- 3 Abstracts in scientific meeting (*see Addendum 4*):
    - 1 poster presentation
    - 2 oral communications
- 1 Manuscript in preparation
- A set of 62 pure and analyzed (IR, 1H-NMR, 13C NMR, physical constants and elementary analysis) molecules available for biological assays (*see Addendum 3*)
- A method for concentrating DENV1 from patient plasma.
- A method for DENV1 fusion inhibitor screening

Conclusion

During this first year of funding, we were able to take over the primary results of a virtual HTS campaign providing a set of potential hit compounds targeting DENV2 βOG binding site. We identify, and acquire a fully chemically characterized diverse set of compounds with potential bioactivity as DENV fusion inhibitors. We have established valid bioassay to screen DENV1 fusion inhibitors, and we are in the process of biological evaluation of the selected compounds. However, based in our current accomplishment of projects goals we are requesting a 3 month extension to accomplish all statement of work goals.

References

1. Halstead, S. B. Dengue. *The Lancet* **2007,** 370, 1644-1652.
2. Morens, D. M.; Fauci, A. S. Dengue and hemorrhagic fever: a potential threat to public health in the United States. *JAMA* **2008,** 299, 214-6.
3. Stephenson, J. R. Understanding dengue pathogenesis: implications for vaccine design. *Bull World Health Organ* **2005,** 83, 308-14.
4. Chaturvedi, U. C.; Shrivastava, R.; Nagar, R. Dengue vaccines: problems and prospects. *Indian J Med Res* **2005,** 121, 639-52.
5. Whitehead, S. S.; Blaney, J. E.; Durbin, A. P.; Murphy, B. R. Prospects for a dengue virus vaccine. *Nat Rev Micro* **2007,** 5, 518-528.
6. Sampath, A.; Padmanabhan, R. Molecular targets for flavivirus drug discovery. *Antiviral Res* **2009,** 81, 6-15.
7. Perera, R.; Khaliq, M.; Kuhn, R. J. Closing the door on flaviviruses: entry as a target for antiviral drug design. *Antiviral Res* **2008,** 80, 11-22.
8. Acosta, E. G.; Talarico, L. B.; Damonte, E. B. Cell entry of dengue virus. *Future Virology* **2008,** 3, 471-479.
9. Kuhn, R. J.; Zhang, W.; Rossmann, M. G.; Pletnev, S. V.; Corver, J.; Lenches, E.; Jones, C. T.; Mukhopadhyay, S.; Chipman, P. R.; Strauss, E. G.; Baker, T. S.; Strauss, J. H. Structure of dengue virus: implications for flavivirus organization, maturation, and fusion. *Cell* **2002,** 108, 717-25.
10. Stiasny, K.; Brandler, S.; Kossl, C.; Heinz, F. X. Probing the flavivirus membrane fusion mechanism by using monoclonal antibodies. *J Virol* **2007,** 81, 11526-31.
11. Stiasny, K.; Heinz, F. X. Flavivirus membrane fusion. *J Gen Virol* **2006,** 87, 2755-66.
12. Modis, Y.; Ogata, S.; Clements, D.; Harrison, S. C. A ligand-binding pocket in the dengue virus envelope glycoprotein. *Proc Natl Acad Sci U S A* **2003,** 100, 6986-91.
13. McKinlay, M. A. Discovery and development of antipicornaviral agents. *Scand J Infect Dis Suppl* **1993,** 88, 109-15.
14. Giranda, V. L. Structure-based drug design of antirhinoviral compounds. *Structure* **1994,** 2, 695-8.
15. Joseph-McCarthy, D.; Hogle, J. M.; Karplus, M. Use of the multiple copy simultaneous search (MCSS) method to design a new class of picornavirus capsid binding drugs. *Proteins* **1997,** 29, 32-58.
16. Charles, C. H.; Yelmene, M.; Luo, G. X. Recent advances in rhinovirus therapeutics. *Curr Drug Targets Infect Disord* **2004,** 4, 331-7.
17. Stultz, C. M.; Karplus, M. MCSS functionality maps for a flexible protein. *Proteins* **1999,** 37, 512-29.
18. Inte:Ligand. Ilib diverse version 1.02. *Inte:Ligand GmbH:* **2006**.
19. Wichmann, O.; Jelinek, T. Dengue in travelers: a review. *J Travel Med* **2004,** 11, 161-70.
20. Wilder-Smith, A.; Schwartz, E. Dengue in travelers. *N Engl J Med* **2005,** 353, 924-32.
21. Kielian, M. Class II virus membrane fusion proteins. *Virology* **2006,** 344, 38-47.
22. Abraham, M. H.; Le, J. The correlation and prediction of the solubility of compounds in water using an amended solvation energy relationship. *J Pharm Sci* **1999,** 88, 868-80.
23. Misra, U. K.; Kalita, J.; Syam, U. K.; Dhole, T. N. Neurological manifestations of dengue virus infection. *J Neurol Sci* **2006,** 244, 117-22.
24. Solomon, T. Flavivirus encephalitis. *N Engl J Med* **2004,** 351, 370-8.
25. Hitchcock, S. A.; Pennington, L. D. Structure-brain exposure relationships. *J Med Chem* **2006,** 49, 7559-83.
26. Wang, Q.-Y.; Patel, S. J.; Vangrevelinghe, E.; Xu, H. Y.; Rao, R.; Jaber, D.; Schul, W.; Gu, F.; Heudi, O.; Ma, N. L.; Poh, M. K.; Phong, W. Y.; Keller, T. H.; Jacoby, E.; Vasudevan, S. G. A Small Molecule Dengue Virus Entry Inhibitor. *Antimicrob. Agents Chemother.* **2009**, AAC.01148-08.
27. Yang, J. M.; Chen, Y. F.; Tu, Y. Y.; Yen, K. R.; Yang, Y. L. Combinatorial computational approaches to identify tetracycline derivatives as flavivirus inhibitors. *PLoS ONE* **2007,** 2, e428.
28. Yennamalli, R.; Subbarao, N.; Kampmann, T.; McGeary, R. P.; Young, P. R.; Kobe, B. Identification of novel target sites and an inhibitor of the dengue virus E protein. *J Comput Aided Mol Des* **2009**.
29. Zhou, Z.; Khaliq, M.; Suk, J. E.; Patkar, C.; Li, L.; Kuhn, R. J.; Post, C. B. Antiviral compounds discovered by virtual screening of small-molecule libraries against dengue virus E protein. *ACS Chem Biol* **2008,** 3, 765-75.
30. Li, Z.; Khaliq, M.; Zhou, Z.; Post, C. B.; Kuhn, R. J.; Cushman, M. Design, synthesis, and biological evaluation of antiviral agents targeting flavivirus envelope proteins. *J Med Chem* **2008,** 51, 4660-71.

APPENDIX

List of Personnel Receiving Pay from the Research Effort

Carlos F. Lagos, Pharmaceutical Chemist, Research Scientist Assistant
Fernando Valiente, Biochemist, Research Scientist Assistant

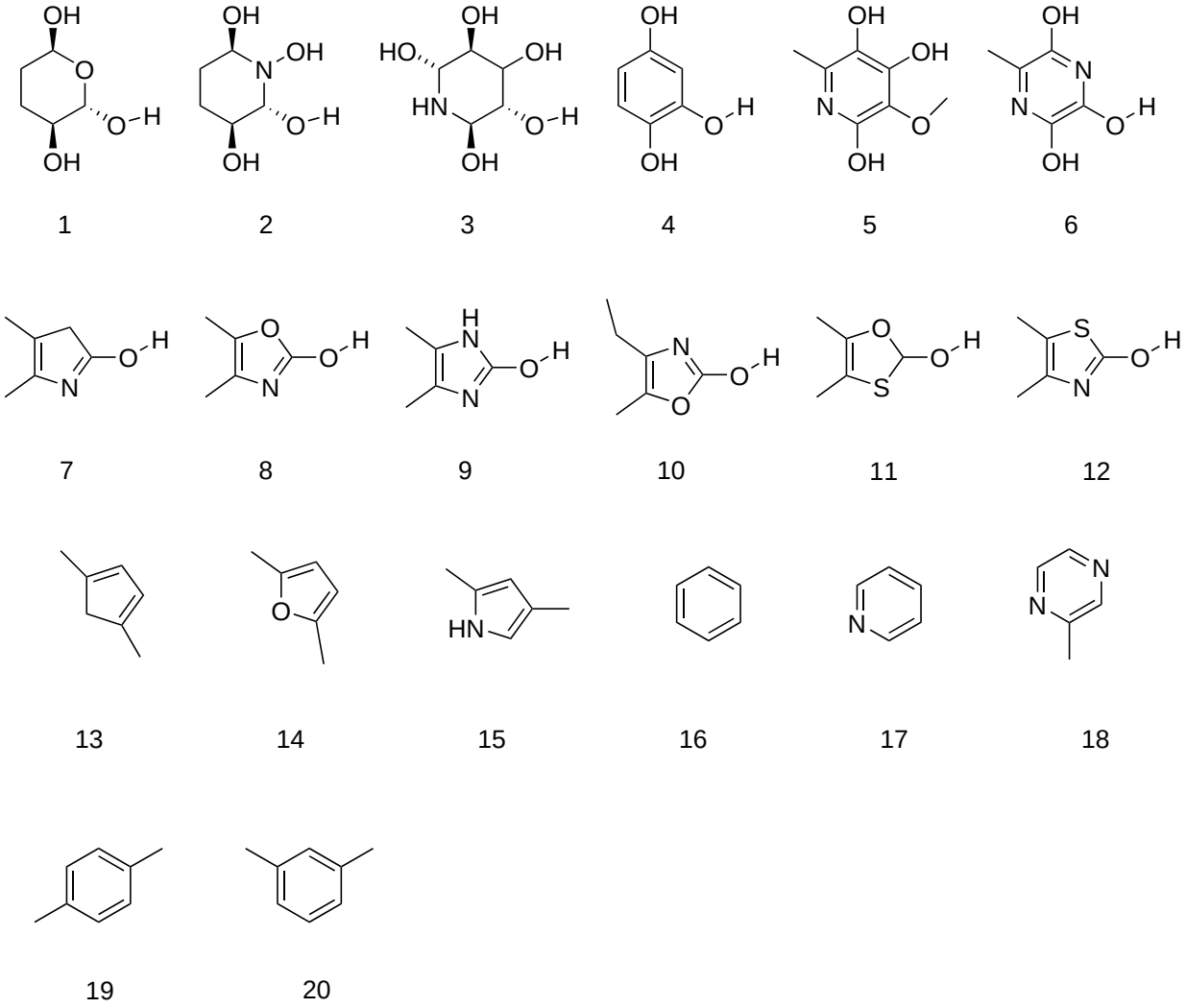

Figure 1. Structure of fragments used in functional group mapping.

Table 1 Molegro Virtual Docker Binding Energies for Functional Groups.

Name	Ligand	MolDockScore	Affinity	Rerank Score	Interaction	Protein	Internal
BOG	**BOG (1OKE)**	**-279.601**	**-113.251**	**-298.703**	**-708.415**	**-708.415**	**428.814**
Name	**Ligand**	**MolDockScore**	**Affinity**	**Rerank Score**	**Interaction**	**Protein**	**Internal**
ACAM	[00] ACAM	-492.128	-202.089	-378.618	-515.288	-515.288	231.595
ACAM	[04] ACAM	-40,92	-189.337	-361.953	-432.352	-432.352	231.516
ACAM	[01] ACAM	-397.713	-203.124	-353.067	-420.865	-420.865	231.524
ACAM	[06] ACAM	-388.467	-194.095	195.592	-411.619	-411.619	231.518
ACAM	[03] ACAM	-387.353	-206.815	-347.409	-410.511	-410.511	231.584
ACAM	[09] ACAM	-375.472	-208.367	-321.745	-398.632	-398.632	231.597
ACAM	[07] ACAM	-371.266	-19.423	-330.067	-394.418	-394.418	231.523
ACAM	[02] ACAM	-366.859	-192.852	-31.233	-390.015	-390.015	231.565
ACAM	[05] ACAM	-364.108	-194.434	-319.061	-387.261	-387.261	231.534
ACAM	[08] ACAM	-331.534	-184.904	-303.251	-354.692	-354.692	231.577
ARGR	[00] ARGR	-585.628	-191.193	-389.076	-587.591	-587.591	0,19628
ARGR	[03] ARGR	-553.725	-19.294	-47.136	-576.896	-576.896	231.709
ARGR	[05] ARGR	-489.538	-19,35	-407.395	-555.467	-555.467	659.288
ARGR	[01] ARGR	-476.984	-168.206	-391.215	-549.208	-549.208	722.248
ARGR	[02] ARGR	-478.579	-168.893	-381.501	-539.123	-539.123	605.433
ARGR	[08] ARGR	-46,95	-180.665	-364.218	-535.661	-535.661	661.616
ARGR	[04] ARGR	-453.194	-153.863	-35,21	-514.403	-514.403	612.092
ARGR	[07] ARGR	-489.365	-167.297	-403.985	-509.152	-509.152	19.787
ARGR	[06] ARGR	-409.176	-150.722	-326.045	-475.635	-475.635	664.588
ARGR	[09] ARGR	-378.174	-149.184	-287.548	-432.948	-432.948	547.736
BZOXZ	[00] BZOXZ	-534.717	-255.284	-413.528	-586.277	-586.277	5.156
BZOXZ	[03] BZOXZ	-532.276	-243.711	-448.901	-583.828	-583.828	515.523
BZOXZ	[05] BZOXZ	-518.181	-243.681	-431.382	-569.739	-569.739	515.577
BZOXZ	[07] BZOXZ	-513.986	-243.677	-424.006	-565.531	-565.531	515.447
BZOXZ	[02] BZOXZ	-504.581	-243.678	-437.128	-556.129	-556.129	515.483
BZOXZ	[09] BZOXZ	-503.379	-243.678	-365.885	-554.927	-554.927	515.483
BZOXZ	[06] BZOXZ	-47.938	-243.681	-406.799	-530.936	-530.936	515.561
BZOXZ	[04] BZOXZ	-567.111	-260.382	-475.617	-61.867	-61.867	515.594
BZOXZ	[08] BZOXZ	-491.487	-243.811	-41.857	-54.304	-54.304	515.535
BZOXZ	[01] BZOXZ	-536.048	-245.833	-459.542	-58,76	-58,76	515.524
BZTF	[00] BZTF	-539.765	-243.647	-45.547	-589.486	-589.486	497.213
BZTF	[01] BZTF	-536.363	-243.719	-449.434	-586.077	-586.077	497.136
BZTF	[03] BZTF	-528.224	-243.451	-438.296	-577.946	-577.946	49.722
BZTF	[02] BZTF	-527.662	-243.447	-448.131	-577.374	-577.374	497.121
BZTF	[04] BZTF	-509.766	-243.449	-419.243	-559.485	-559.485	497.192
BZTF	[05] BZTF	-502.694	-243.448	-440.797	-552.412	-552.412	49.718
BZTF	[08] BZTF	-499.127	-243.447	-413.395	-548.841	-548.841	497.139
BZTF	[09] BZTF	-491.779	-243.451	-417.023	-541.502	-541.502	497.233
BZTF	[07] BZTF	-490.189	-243.448	-420.296	-539.907	-539.907	497.182
BZTF	[06] BZTF	-487.854	-254.755	-430.341	-537.573	-537.573	497.195
CPENT	[00] CPENT	-491.633	-195.693	-342.799	-491.633	-491.633	0
CPENT	[02] CPENT	-488.999	-195.693	-354.309	-488.999	-488.999	0
CPENT	[03] CPENT	-464.938	-195.693	-378.768	-464.938	-464.938	0
CPENT	[04] CPENT	-452.679	-195.693	-362.647	-452.679	-452.679	0

CPENT	[06] CPENT	-441.001	-195.693	-34.006	-441.001	-441.001	0
CPENT	[05] CPENT	-439.207	-195.693	-350.562	-439.207	-439.207	0
CPENT	[09] CPENT	-428.775	-195.693	-820.051	-428.775	-428.775	0
CPENT	[01] CPENT	-49.038	-195.693	-346.139	-49.038	-49.038	0
CPENT	[08] CPENT	-43.467	-195.693	-307.666	-43.467	-43.467	0
CPENT	[07] CPENT	-43.423	-195.693	-307.282	-43.423	-43.423	0
CPENTEN	[00] CPENTEN	-452.014	-195.693	-344.031	-452.014	-452.014	0
CPENTEN	[01] CPENTEN	-381.646	-195.693	-320.928	-381.646	-381.646	0
CPENTEN	[02] CPENTEN	-371.484	-195.693	-210.076	-371.484	-371.484	0
CPENTEN	[03] CPENTEN	-365.592	-195.693	-135.315	-365.592	-365.592	0
CPENTEN	[04] CPENTEN	-358.382	-195.693	-289.626	-358.382	-358.382	0
CPENTEN	[05] CPENTEN	-356.878	-195.693	-303.481	-356.878	-356.878	0
CPENTEN	[06] CPENTEN	-350.121	-195.693	-19,84	-350.121	-350.121	0
CPENTEN	[07] CPENTEN	-338.962	-195.693	-289.137	-338.962	-338.962	0
CPENTEN	[08] CPENTEN	-334.806	-195.693	-282.529	-334.806	-334.806	0
CPENTEN	[09] CPENTEN	-332.272	-195.693	-285.444	-332.272	-332.272	0
DMBENZ	[00] DMBENZ	-482.391	-200.943	-420.308	-544.752	-544.752	62.361
DMBENZ	[01] DMBENZ	-474.285	-200.943	-39.549	-536.645	-536.645	623.601
DMBENZ	[02] DMBENZ	-451.603	-200.942	-393.482	-513.961	-513.961	623.579
DMBENZ	[03] DMBENZ	-442.224	-200.944	-383.988	-504.589	-504.589	623.645
DMBENZ	[04] DMBENZ	-433.456	-200.943	-373.281	-495.817	-495.817	623.609
DMBENZ	[05] DMBENZ	-426.572	-200.944	-35.126	-488.937	-488.937	623.649
DMBENZ	[07] DMBENZ	-41.682	-20.094	-317.276	-479.175	-479.175	623.546
DMBENZ	[08] DMBENZ	-413.793	-200.944	-354.948	-476.158	-476.158	623.647
DMBENZ	[09] DMBENZ	-413.186	-200.947	-366.071	-475.559	-475.559	623.729
DMBENZ	[06] DMBENZ	-419.805	-200.944	-284.905	-48.217	-48.217	623.648
FUR	[00] FUR	-505.248	-232.423	-395.194	-505.248	-505.248	0
FUR	[01] FUR	-497.421	-22.934	-404.353	-497.421	-497.421	0
FUR	[02] FUR	-476.309	-23.299	-219.583	-476.309	-476.309	0
FUR	[03] FUR	-472.606	-220.821	-259.486	-472.606	-472.606	0
FUR	[04] FUR	-462.716	-232.423	-357.194	-462.716	-462.716	0
FUR	[06] FUR	-451.028	-232.125	-35.374	-451.028	-451.028	0
FUR	[07] FUR	-440.254	-220.821	-369.087	-440.254	-440.254	0
FUR	[09] FUR	-435.908	-220.821	-33.637	-435.908	-435.908	0
FUR	[08] FUR	-43.768	-220.821	-352.101	-43.768	-43.768	0
FUR	[05] FUR	-46	-220.821	-340.607	-46	-46	0
GLNR	[01] GLNR	-510.125	-20.874	-404.348	-521.691	-521.691	115.666
GLNR	[02] GLNR	-49.911	-222.574	-430.552	-510.565	-510.565	114.548
GLNR	[00] GLNR	-486.336	-214.383	-214.383	-500.992	-500.992	146.561
GLNR	[04] GLNR	-473.746	-201.209	-192.368	-486.146	-486.146	1,24
GLNR	[03] GLNR	-473.046	-218.665	-410.354	-483.649	-483.649	106.026
GLNR	[05] GLNR	-460.965	-217.563	-39.985	-472.392	-472.392	114.271
GLNR	[07] GLNR	-449.842	-22.277	-382.051	-460.349	-460.349	105.068
GLNR	[08] GLNR	-436.113	-220.034	-379.224	-455.054	-455.054	189.414
GLNR	[09] GLNR	-429.808	-217.948	-368.184	-443.043	-443.043	132.349
GLNR	[06] GLNR	-455.681	-220.465	-389.025	-47.127	-47.127	155.896
HISR	[00] HISR	-483.842	-213.489	-415.563	-475.875	-475.875	-0,796707

HISR	[01] HISR	-455.675	-214.875	-389.241	-447.708	-447.708	-0,79669
HISR	[08] HISR	-455.431	-215.749	-379.061	-447.464	-447.464	-0,796751
HISR	[04] HISR	-442.641	-206.212	-381.508	-434.672	-434.672	-0,79686
HISR	[05] HISR	-438.767	-199.046	-371.295	-430.799	-430.799	-0,796849
HISR	[03] HISR	-413.083	-200.071	-345.269	-405.115	-405.115	-0,79676
HISR	[09] HISR	-411.796	-204.142	-349.773	-403.828	-403.828	-0,796806
HISR	[02] HISR	-410.256	-199.046	-341.488	-402.288	-402.288	-0,796761
HISR	[07] HISR	-401.399	-212.246	-328.059	-393.431	-393.431	-0,79682
HISR	[06] HISR	-397.641	-201.711	-330.496	-389.673	-389.673	-0,79677
IMID	[00] IMID	-542.958	-204.726	-442.355	-542.958	-542.958	0
IMID	[02] IMID	-514.753	-210.135	-397.521	-514.753	-514.753	0
IMID	[03] IMID	-506.987	-211.429	-294.898	-506.987	-506.987	0
IMID	[01] IMID	-503.568	-20.539	-399.349	-503.568	-503.568	0
IMID	[05] IMID	-491.809	-211.429	-404.854	-491.809	-491.809	0
IMID	[04] IMID	-466.267	-201.137	-115.895	-466.267	-466.267	0
IMID	[06] IMID	-465.052	-199.828	-168.937	-465.052	-465.052	0
IMID	[09] IMID	-451.696	-199.828	-369.554	-451.696	-451.696	0
IMID	[07] IMID	-438.185	-203.908	-296.161	-438.185	-438.185	0
IMID	[08] IMID	-43.994	-199.828	-338.723	-43.994	-43.994	0
INDOL	[04] INDOL	-537.188	-223.811	-458.889	-588.754	-588.754	515.664
INDOL	[07] INDOL	-536.469	-223.006	-451.661	-588.019	-588.019	515.503
INDOL	[05] INDOL	-536.204	-224.051	-449.433	-587.762	-587.762	515.582
INDOL	[02] INDOL	-533.993	-231.961	-455.828	-585.555	-585.555	515.617
INDOL	[01] INDOL	-530.658	-228.299	-457.232	-582.221	-582.221	515.636
INDOL	[09] INDOL	-499.659	-22.268	-426.634	-551.215	-551.215	515.557
INDOL	[06] INDOL	-497.044	-222.682	-406.237	-548.609	-548.609	515.648
INDOL	[00] INDOL	-488.239	-224.346	-400.401	-539.803	-539.803	515.642
INDOL	[03] INDOL	-505.038	-237.807	-380.519	-55.659	-55.659	51.552
INDOL	[08] INDOL	-484.305	-226.974	-34,77	-53.586	-53.586	515.549
MDHP	[01] MDHP	-434.882	-20.887	-390.185	-503.616	-503.616	687.341
MDHP	[02] MDHP	-42.643	-210.617	-30.902	-495.163	-495.163	687.335
MDHP	[00] MDHP	-419.442	-200.096	-381.317	-488.166	-488.166	687.239
MDHP	[04] MDHP	-411.303	-199.015	-360.083	-480.031	-480.031	687.285
MDHP	[03] MDHP	-392.636	-211.722	-330.047	-461.365	-461.365	687.288
MDHP	[09] MDHP	-390.983	-204.097	-349.078	-459.715	-459.715	687.323
MDHP	[08] MDHP	-386.883	-202.792	-355.227	-455.612	-455.612	687.289
MDHP	[05] MDHP	-383.872	-199.016	-345.173	-452.607	-452.607	68.735
MDHP	[06] MDHP	-368.638	-200.384	-278.605	-437.364	-437.364	687.263
MDHP	[07] MDHP	-383.334	-199.014	-340.829	-45.206	-45.206	687.258
MORPH	[00] MORPH	-378.346	-233.585	-34.665	-453.928	-453.928	755.814
MORPH	[02] MORPH	-362.132	-218.906	-336.939	-437.713	-437.713	755.812
MORPH	[04] MORPH	-355.537	-220.046	-339.505	-431.122	-431.122	755.842
MORPH	[05] MORPH	-351.118	-22.072	-338.293	-426.698	-426.698	755.801
MORPH	[01] MORPH	-343.544	-217.652	-327.513	-419.129	-419.129	755.848
MORPH	[03] MORPH	-339.305	-220.722	-317.942	-414.889	-414.889	755.835
MORPH	[07] MORPH	-337.799	-218.587	-318.249	-413.378	-413.378	755.798
MORPH	[09] MORPH	-329.864	-220.721	-272.208	-405.443	-405.443	755.783

MORPH	[06] MORPH	-325.577	-22.426	-322.721	-401.165	-401.165	755.878
MORPH	[08] MORPH	-29.864	-22.905	-137.965	-374.226	-374.226	755.865
MORPH	MORPH	148.277	-20.912	100.134	72.691	0	755.859
OXZ	[05] OXZ	-540.862	-243.801	-44.671	-540.862	-540.862	0
OXZ	[00] OXZ	-493.236	-236.558	-382.711	-493.236	-493.236	0
OXZ	[03] OXZ	-465.409	-229.802	-380.811	-465.409	-465.409	0
OXZ	[04] OXZ	-440.075	-236.558	-301.623	-440.075	-440.075	0
OXZ	[08] OXZ	-437.919	-228.154	-335.893	-437.919	-437.919	0
OXZ	[06] OXZ	-432.656	-236.545	-222.809	-432.656	-432.656	0
OXZ	[09] OXZ	-425.408	-230.614	-320.476	-425.408	-425.408	0
OXZ	[01] OXZ	-424.853	-225.525	-340.582	-424.853	-424.853	0
OXZ	[07] OXZ	-405.524	-224.956	-339.642	-405.524	-405.524	0
OXZ	[02] OXZ	-48.597	-236.405	-403.569	-48.597	-48.597	0
PHEN	[04] PHEN	-389.161	-200.312	-34.983	-465.097	-465.097	759.358
PHEN	[02] PHEN	-385.278	-200.313	-349.681	-461.217	-461.217	759.386
PHEN	[01] PHEN	-368.968	-201.444	-33.945	-444.902	-444.902	759.334
PHEN	[07] PHEN	-36.575	-204.783	-331.219	-441.686	-441.686	759.359
PHEN	[00] PHEN	-358.629	-200.375	-33.428	-434.556	-434.556	759.275
PHEN	[09] PHEN	-352.208	-200.308	-302.193	-428.134	-428.134	759.254
PHEN	[03] PHEN	-349.264	-211.912	-266.857	-425.196	-425.196	759.316
PHEN	[05] PHEN	-340.691	-204.643	-318.284	-416.632	-416.632	759.418
PHEN	[08] PHEN	-332.567	-200.316	-28.823	-408.511	-408.511	759.447
PHEN	[06] PHEN	-30.907	-200.312	-290.339	-385.004	-385.004	759.337
PIR	[00] PIR	-399.983	-225.294	-327.434	-499.952	-499.952	999.693
PIR	[05] PIR	-36.193	-23.258	-201.065	-461.896	-461.896	999.654
PIR	[06] PIR	-338.063	-230.698	-308.348	-438.024	-438.024	999.617
PIR	[02] PIR	-335.645	-218.716	703.683	-435.608	-435.608	99.963
PIR	[04] PIR	-299.618	-218.944	-289.274	-399.588	-399.588	9.997
PIR	[01] PIR	-294.588	-218.717	-289.905	-394.553	-394.553	999.651
PIR	[08] PIR	-283.494	-218.715	-266.903	-383.457	-383.457	99.963
PIR	[09] PIR	-280.402	-218.825	184.006	-380.361	-380.361	999.585
PIR	[03] PIR	-26.907	-218.714	-267.177	-369.028	-369.028	999.581
PIR	[07] PIR	-260.078	-21.907	-25.958	-360.043	-360.043	99.965
PPIP	[00] PPIP	-401.755	-176.826	-195.664	-464.087	-464.087	623.328
PPIP	[02] PPIP	-372.263	-18.652	-350.024	-434.591	-434.591	623.282
PPIP	[08] PPIP	-360.528	-176.826	-335.539	-422.864	-422.864	623.362
PPIP	[07] PPIP	-349.211	-179.673	-326.073	-411.544	-411.544	623.337
PPIP	[06] PPIP	-346.269	-179.099	-325.934	-408.595	-408.595	62.327
PPIP	[09] PPIP	-334.973	-17.779	-305.027	-397.307	-397.307	623.335
PPIP	[05] PPIP	-327.223	-188.021	-297.562	-389.558	-389.558	623.346
PPIP	[03] PPIP	-394.831	-188.427	-366.336	-45.716	-45.716	623.295
PPIP	[04] PPIP	-344.612	-184.354	-32.299	-40.694	-40.694	623.277
PPIP	[01] PPIP	-385.675	-186.603	-352.126	-44,8	-44,8	623.251
PYR	[00] PYR	-351.336	-225.008	416.629	-445.507	-445.507	941.708
PYR	[05] PYR	-322.257	-214.469	-306.995	-416.427	-416.427	941.704
PYR	[03] PYR	-319.884	-21.447	-305.135	-414.055	-414.055	941.708
PYR	[01] PYR	-311.863	-214.471	-296.275	-406.036	-406.036	941.733

PYR	[02] PYR	-310.056	-214.469	-297.433	-404.223	-404.223	941.677
PYR	[04] PYR	-305.723	-214.468	-294.333	-399.892	-399.892	941.693
PYR	[07] PYR	-293.353	-215.704	-278.142	-387.525	-387.525	94.173
PYR	[06] PYR	-281.269	-214.471	-275.801	-375.443	-375.443	941.743
PYR	[09] PYR	-267.936	-21.447	-264.268	-362.109	-362.109	94.173
PYR	[08] PYR	-312.109	-214.469	-284.116	-40.628	-40.628	941.703

Table 2. Top 150 Virtual screening results for NCI drug database against Dengue Virus E2 protein.

Index	Structure	Name	Ludi2
1	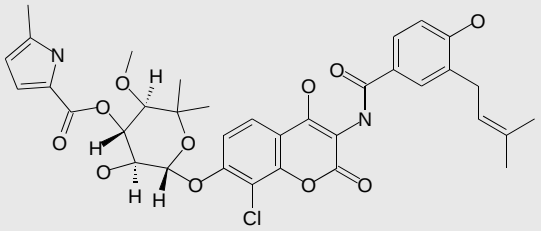	4_227186_1OKE.pdb	724
2	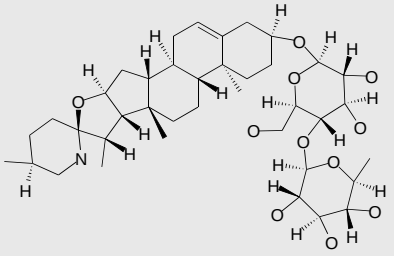	14_376459_1OKE.pdb	678
3	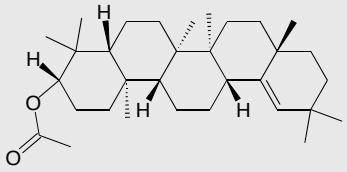	88_403167_1OKE.pdb	639
4	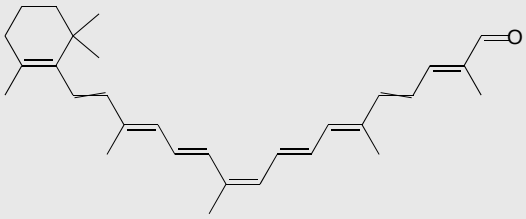	262_374897_1OKE.pdb	638
5	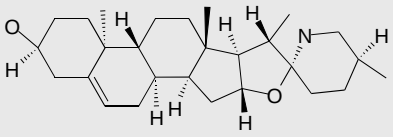	65_178260_1OKE.pdb	628
6	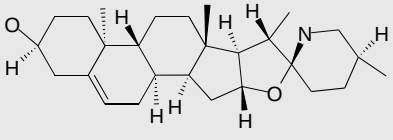	66_179187_1OKE.pdb	628

7	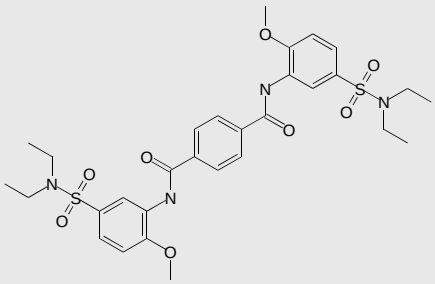	75_111341_1OKE.pdb	627
8	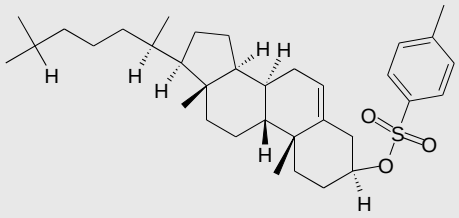	1_134905_1OKE.pdb	623
9	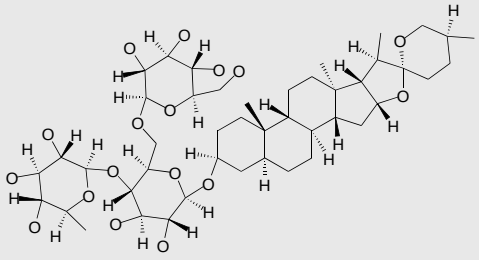	37_104793_1OKE.pdb	619
10	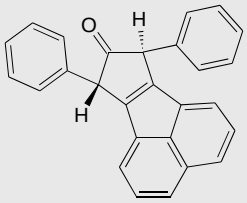	69_627663_1OKE.pdb	554
11	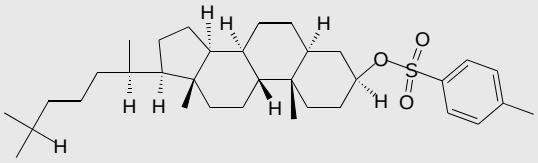	2_132800_1OKE.pdb	592
12	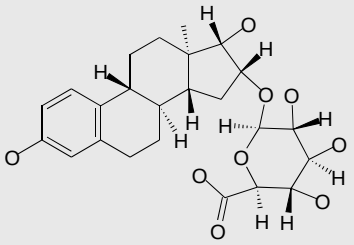	5_93823_1OKE.pdb	397

13	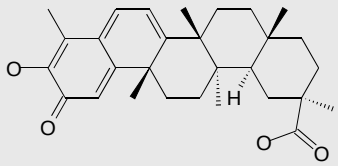	6_70931_1OKE.pdb	526
14	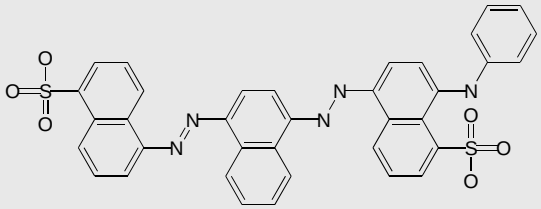	7_47765_1OKE.pdb	510
15	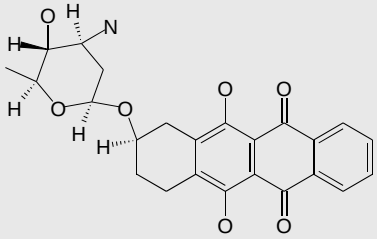	9_262635_1OKE.pdb	398
16	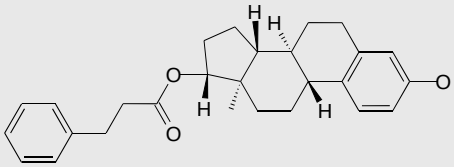	12_26645_1OKE.pdb	547
17	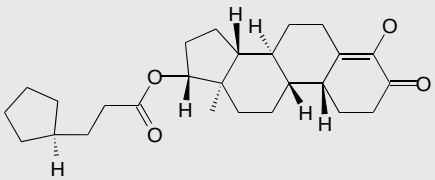	13_522767_1OKE.pdb	526
18	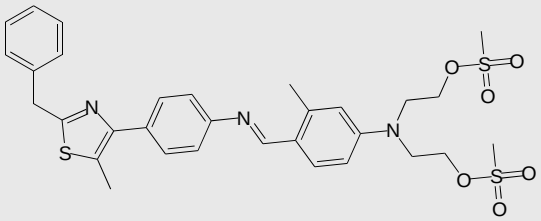	16_281617_1OKE.pdb	576

19	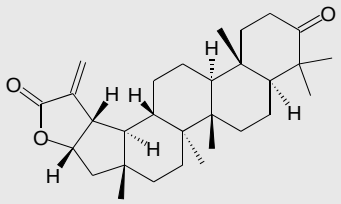	18_680072_1OKE.pdb	528
20	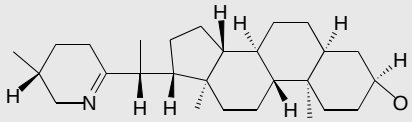	19_87500_1OKE.pdb	569
21	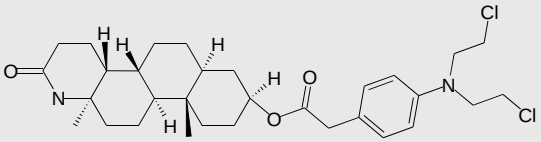	23_620482_1OKE.pdb	543
22	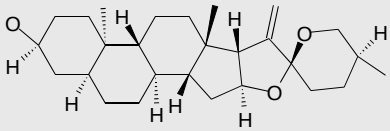	24_1615_1OKE.pdb	549
23	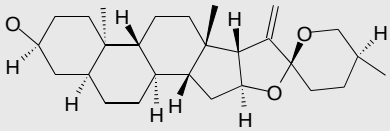	25_93747_1OKE.pdb	553
24	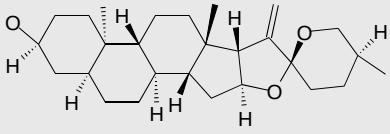	26_93754_1OKE.pdb	549

25	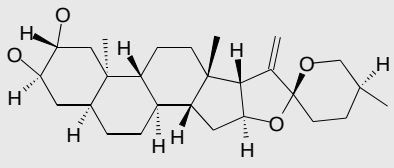	29_147752_1OKE.pdb	468
26	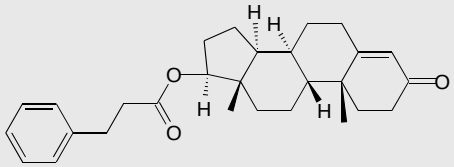	30_26643_1OKE.pdb	597
27	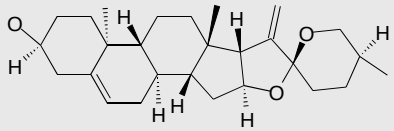	31_226132_1OKE.pdb	542
28	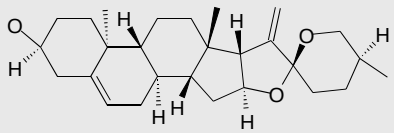	32_33396_1OKE.pdb	542
29	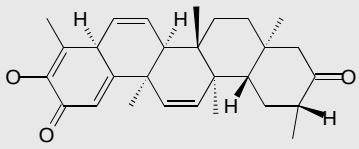	33_608781_1OKE.pdb	524
30	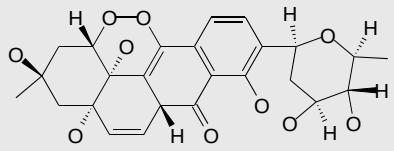	38_184398_1OKE.pdb	422

31	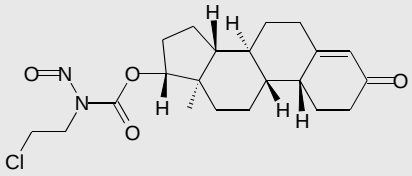	39_269719_1OKE.pdb	445
32	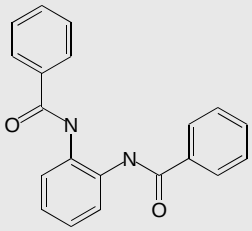	40_81574_1OKE.pdb	468
33	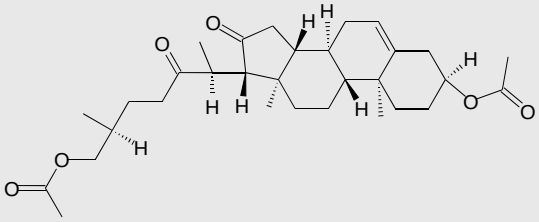	41_226104_1OKE.pdb	537
34	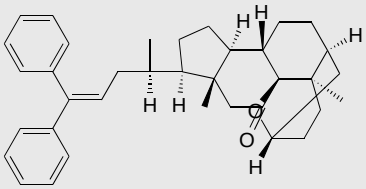	43_45879_1OKE.pdb	588
35	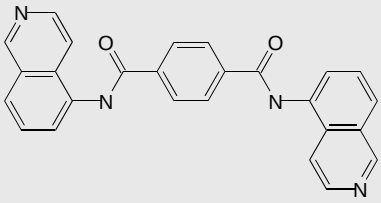	46_111335_1OKE.pdb	507
36	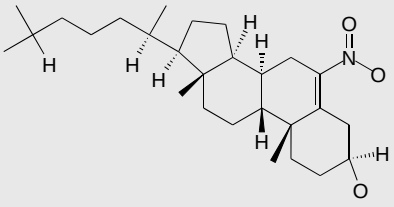	48_128354_1OKE.pdb	519

37	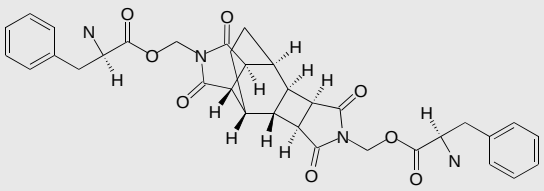	50_373965_1OKE.pdb	457
38	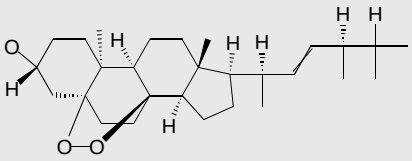	55_31324_1OKE.pdb	515
39	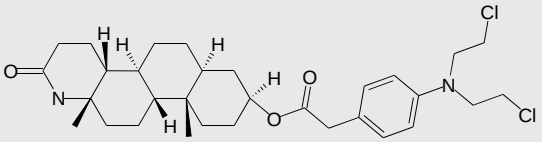	57_290205_1OKE.pdb	530
40	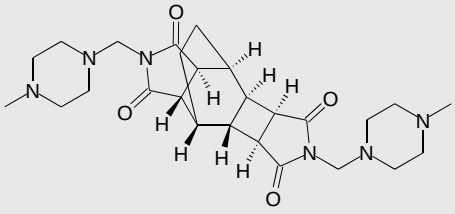	58_364188_1OKE.pdb	541
41	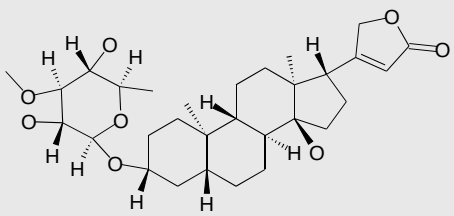	59_123976_1OKE.pdb	506
42	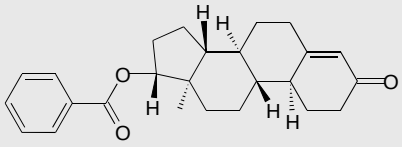	60_19858_1OKE.pdb	541

43	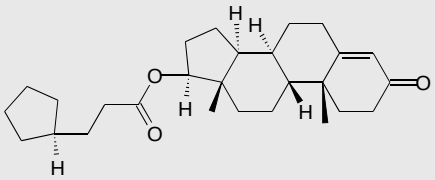	62_9157_1OKE.pdb	495
44	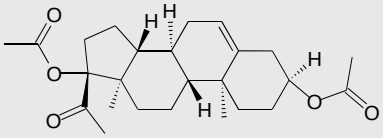	70_107126_1OKE.pdb	519
45	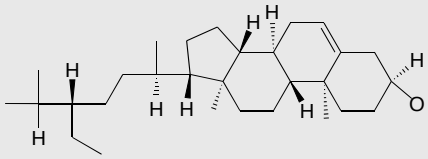	73_8096_1OKE.pdb	467
46	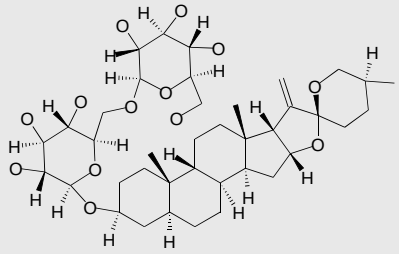	74_104794_1OKE.pdb	595
47	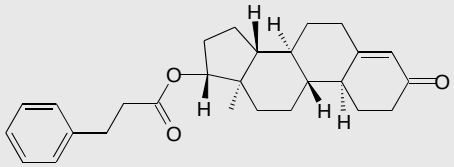	76_23162_1OKE.pdb	520
48	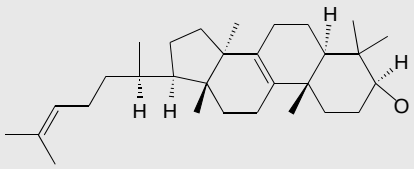	77_403164_1OKE.pdb	568

49	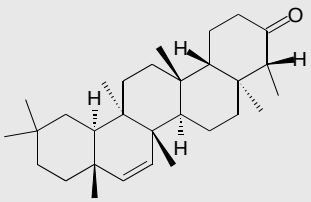	80_55141_1OKE.pdb	540
50	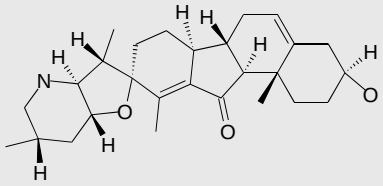	82_23898_1OKE.pdb	542
51	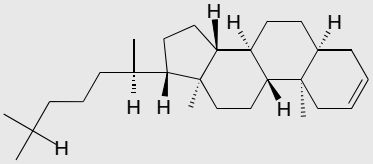	83_119015_1OKE.pdb	514
52	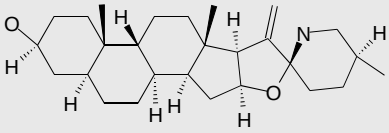	85_27592_1OKE.pdb	522
53	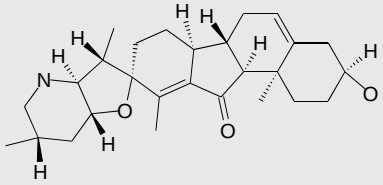	87_7520_1OKE.pdb	567
54	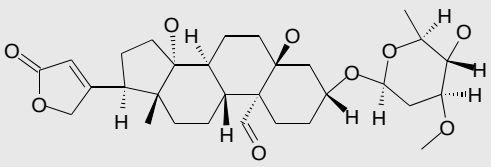	89_7522_1OKE.pdb	450

55	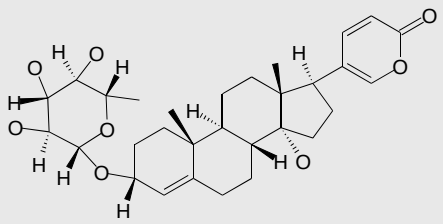	90_7521_1OKE.pdb	552
56	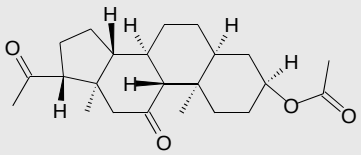	97_60797_1OKE.pdb	471
57	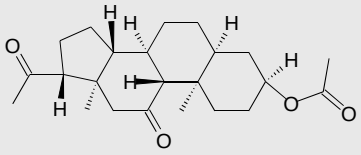	99_73108_1OKE.pdb	471
58	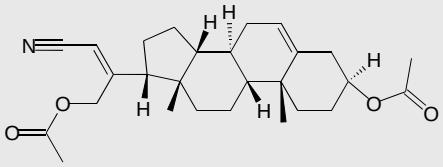	100_121369_1OKE.pdb	535
59	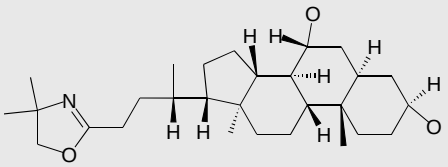	103_606971_1OKE.pdb	416
60	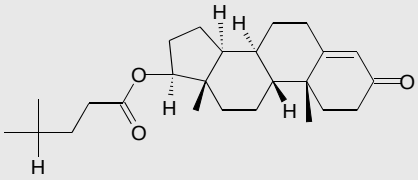	105_26641_1OKE.pdb	506

61	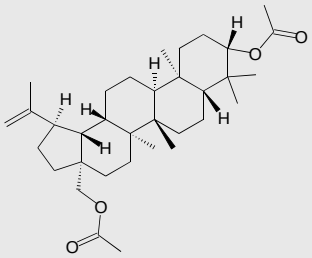	107_38876_1OKE.pdb	537
62	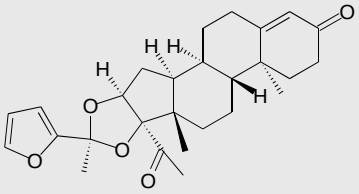	109_72298_1OKE.pdb	425
63	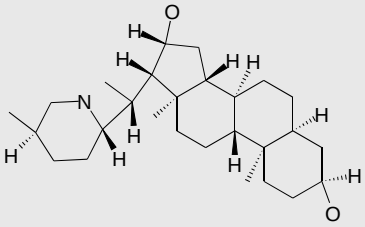	110_96020_1OKE.pdb	440
64	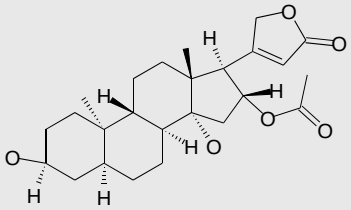	113_148790_1OKE.pdb	442
65	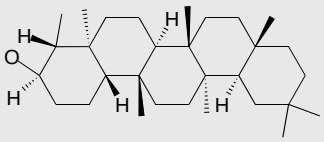	115_407041_1OKE.pdb	552
66	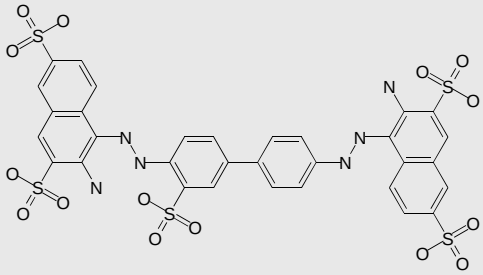	118_11243_1OKE.pdb	418

67	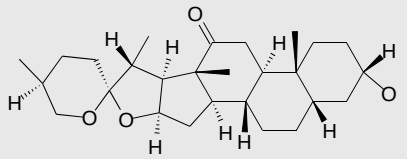	123_115921_1OKE.pdb	530
68	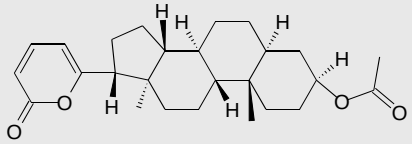	126_114794_1OKE.pdb	535
69	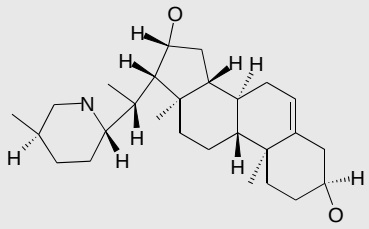	127_224250_1OKE.pdb	513
70	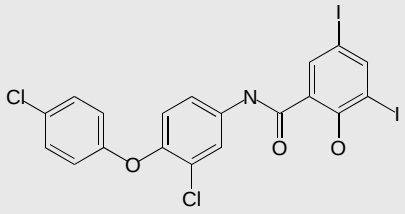	128_355278_1OKE.pdb	459
71	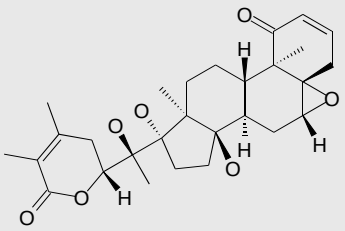	129_179834_1OKE.pdb	445
72	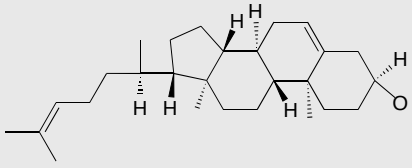	135_226126_1OKE.pdb	476

73	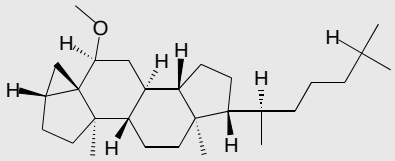	138_134933_1OKE.pdb	573
74	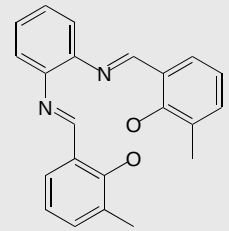	141_51735_1OKE.pdb	551
75	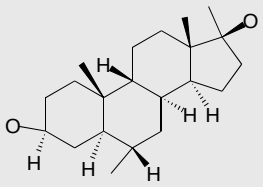	142_58852_1OKE.pdb	463
76	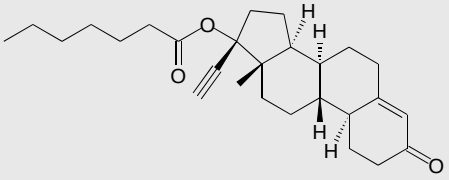	144_22846_1OKE.pdb	460
77	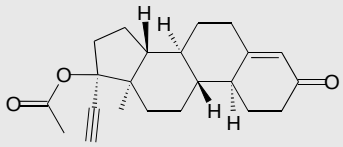	149_22844_1OKE.pdb	481
78	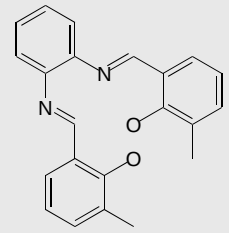	153_51736_1OKE.pdb	547

79	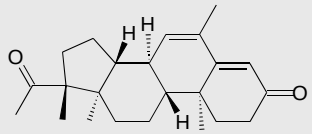	155_123018_1OKE.pdb	477
80	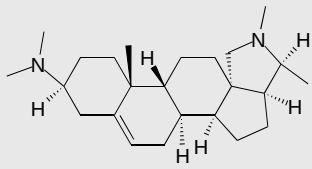	160_347544_1OKE.pdb	568
81	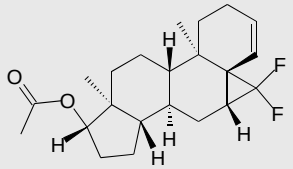	161_94533_1OKE.pdb	493
82	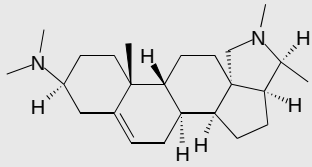	162_17100_1OKE.pdb	568
83	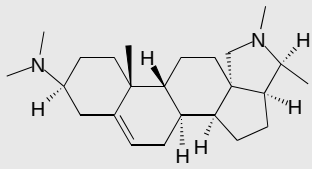	163_32989_1OKE.pdb	568
84	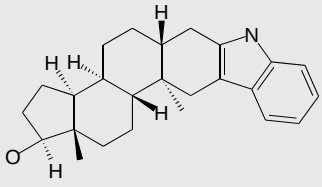	164_60785_1OKE.pdb	524

85	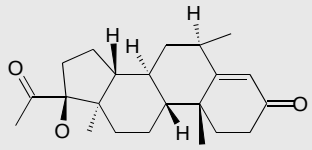	169_27408_1OKE.pdb	398
86	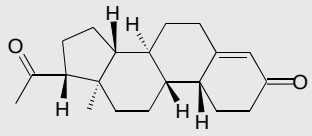	172_22021_1OKE.pdb	420
87	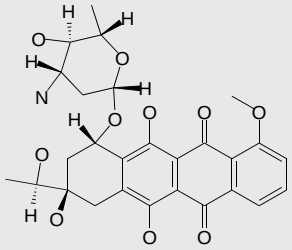	174_180510_1OKE.pdb	392
88	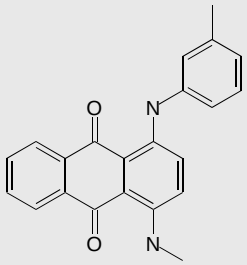	175_297574_1OKE.pdb	493
89	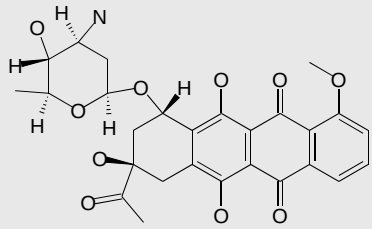	176_304685_1OKE.pdb	345
90	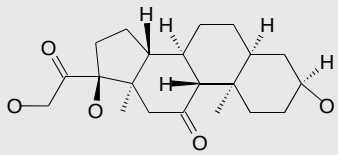	178_76984_1OKE.pdb	338

91	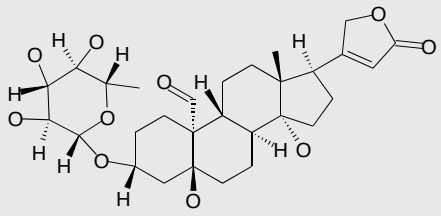	183_407808_1OKE.pdb	363
92	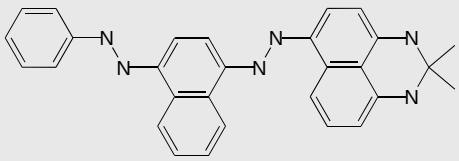	184_11239_1OKE.pdb	594
93	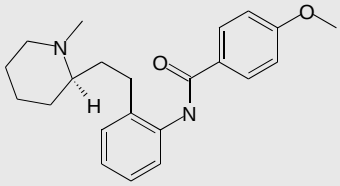	187_299238_1OKE.pdb	557
94	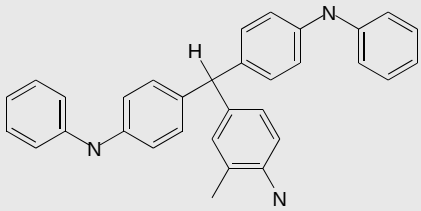	188_8677_1OKE.pdb	511
95	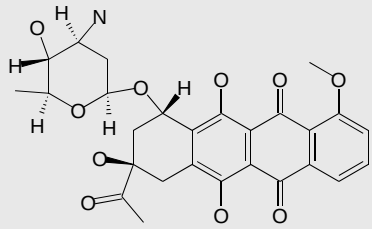	190_301724_1OKE.pdb	346
96	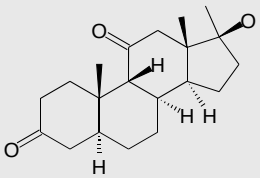	193_19605_1OKE.pdb	418

97	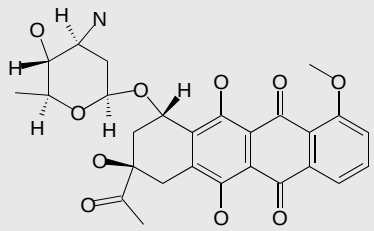	194_262199_1OKE.pdb	339
98	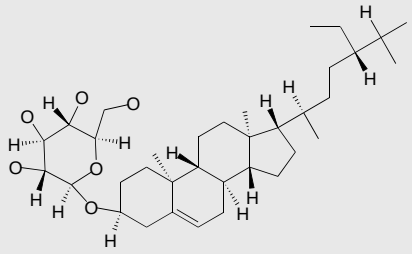	197_165962_1OKE.pdb	532
99	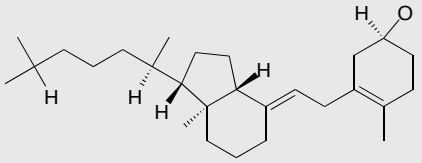	198_375571_1OKE.pdb	572
100	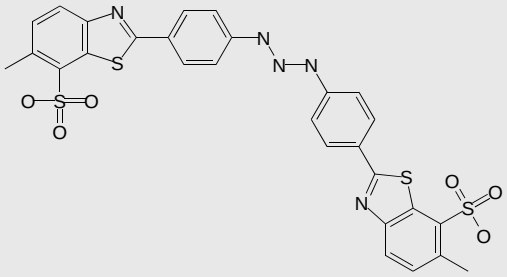	200_47741_1OKE.pdb	491
101	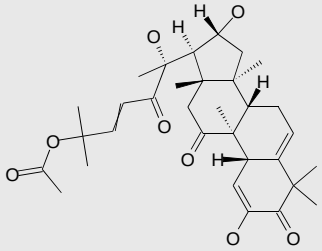	202_106399_1OKE.pdb	449
102	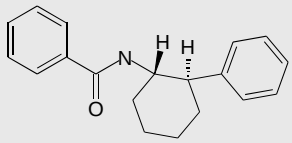	203_122891_1OKE.pdb	534

103	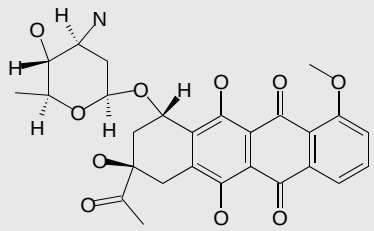	204_303826_1OKE.pdb	389
104	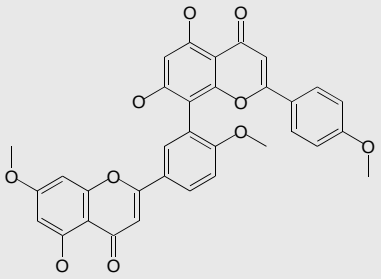	205_45108_1OKE.pdb	537
105	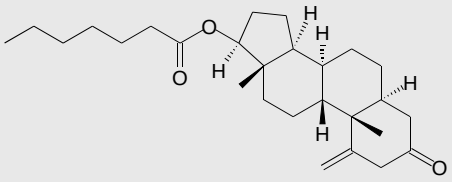	206_64967_1OKE.pdb	498
106	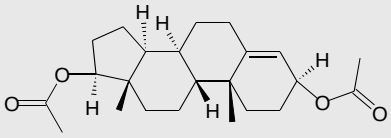	207_11250_1OKE.pdb	502
107	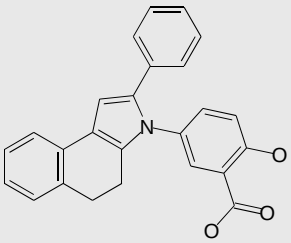	208_351522_1OKE.pdb	385
108	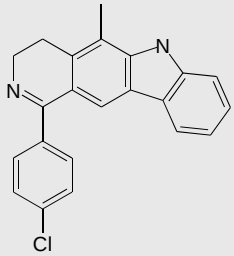	209_83292_1OKE.pdb	561

109	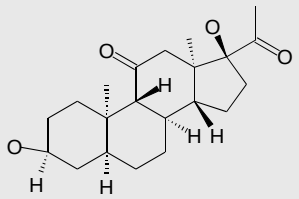	210_82864_1OKE.pdb	385
110	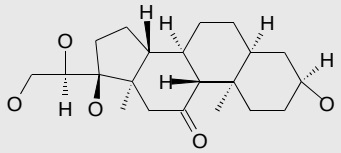	211_59872_1OKE.pdb	325
111	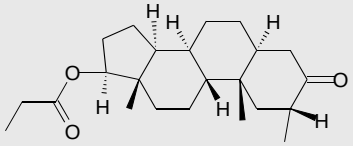	212_12198_1OKE.pdb	467
112	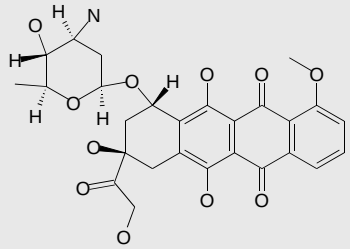	213_302662_1OKE.pdb	295
113	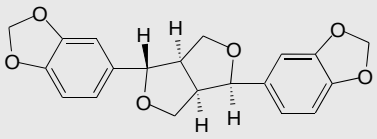	214_31773_1OKE.pdb	394
114	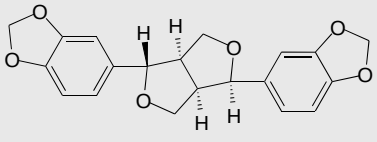	215_36403_1OKE.pdb	394

115	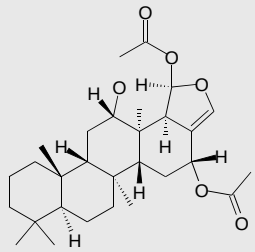	216_369049_1OKE.pdb	431
116	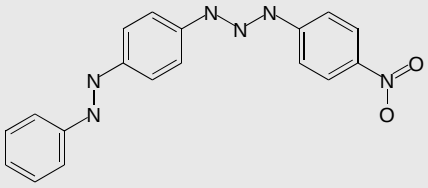	217_66456_1OKE.pdb	422
117	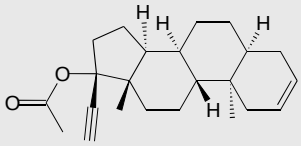	218_69588_1OKE.pdb	525
118	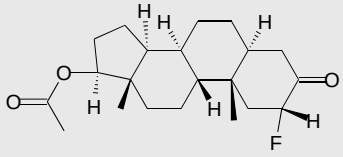	219_73861_1OKE.pdb	477
119	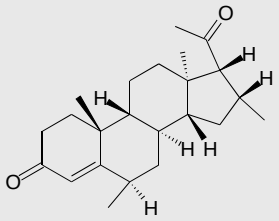	220_103266_1OKE.pdb	431
120	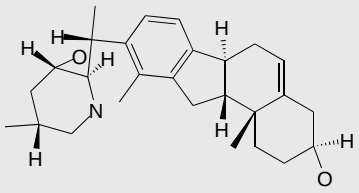	221_17821_1OKE.pdb	433

121	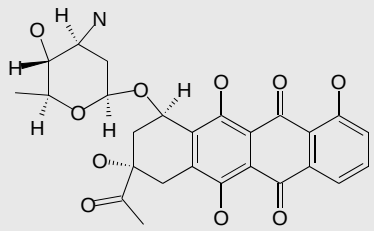	222_180024_1OKE.pdb	320
122	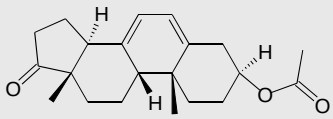	223_226160_1OKE.pdb	477
123	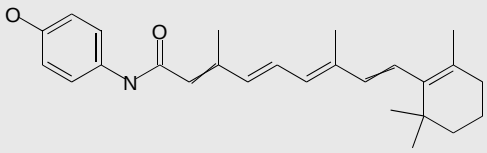	224_374551_1OKE.pdb	584
124	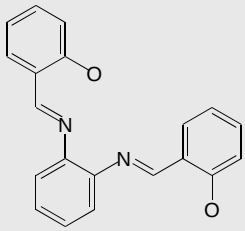	225_51728_1OKE.pdb	483
125	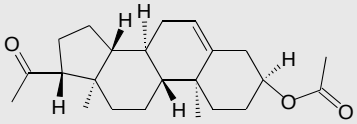	226_64827_1OKE.pdb	481
126	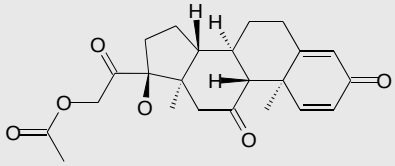	227_10965_1OKE.pdb	428

127	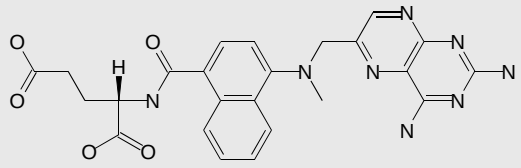	228_174121_1OKE.pdb	236
128	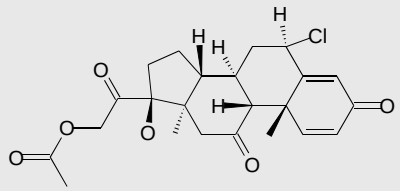	229_37912_1OKE.pdb	395
129	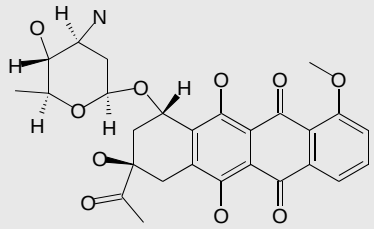	232_272706_1OKE.pdb	391
130	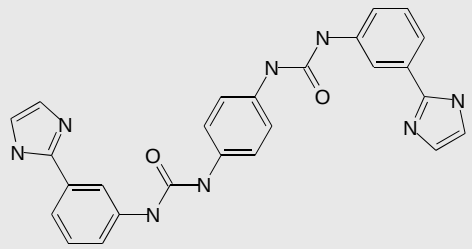	237_57143_1OKE.pdb	524
131	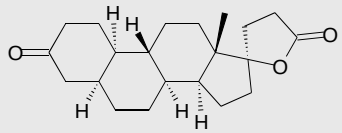	238_61714_1OKE.pdb	451
132	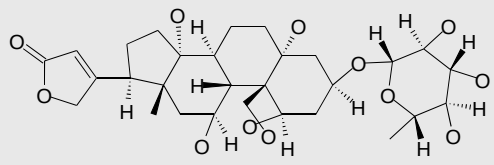	242_25485_1OKE.pdb	352

133	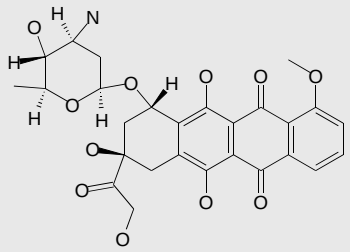	243_256942_1OKE.pdb	304
134	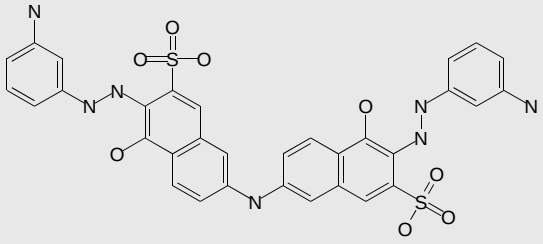	244_58055_1OKE.pdb	455
135	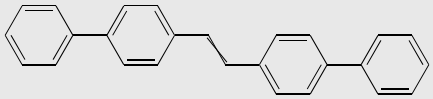	246_88640_1OKE.pdb	507
136	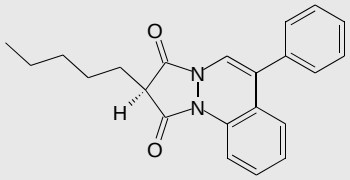	249_102825_1OKE.pdb	422
137	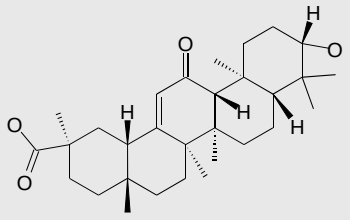	251_35350_1OKE.pdb	520
138	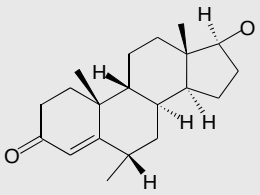	252_38881_1OKE.pdb	439

139	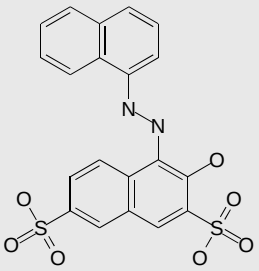	257_45583_1OKE.pdb	284
140	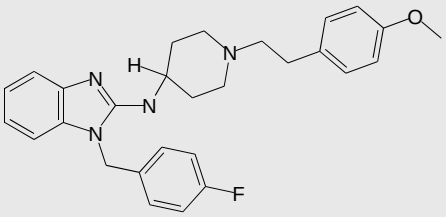	261_329963_1OKE.pdb	488
141	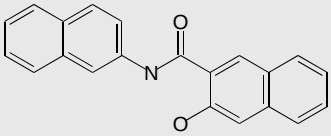	263_42112_1OKE.pdb	441
142	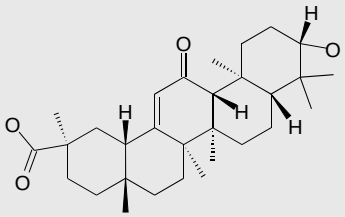	264_35347_1OKE.pdb	524
143	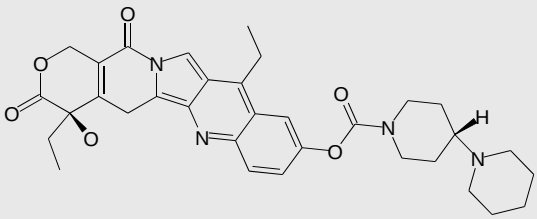	22_616348_1OKE.pdb	579
144	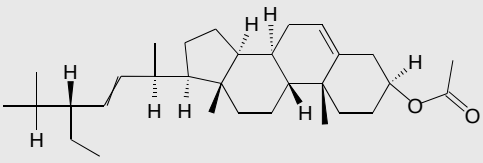	3_8109_1OKE.pdb	584

145	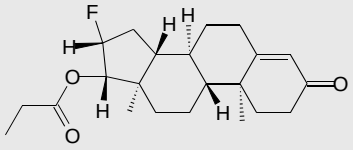	230_56954_1OKE.pdb	450
146	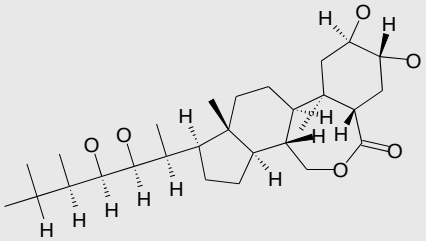	120_325611_1OKE.pdb	467
147	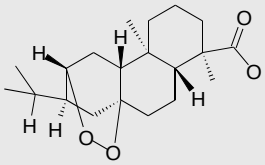	236_406629_1OKE.pdb	457
148	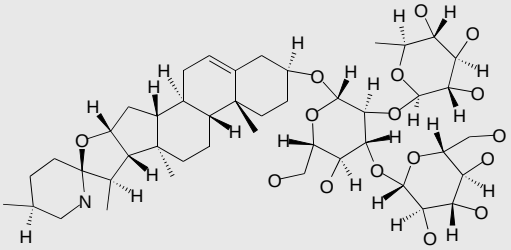	125_82149_1OKE.pdb	610
149	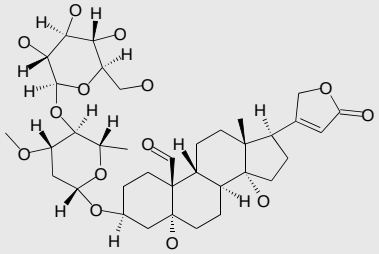	96_4320_1OKE.pdb	408
150	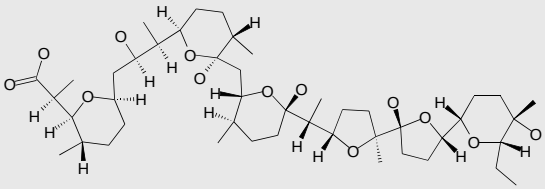	20_177405_1OKE.pdb	453

Table 3. Top 62 compounds identified as broad spectrum dengue virus fusion inhibitors.

Rank	Structure	Name	ShapeIndex	Tanimoto	Shape PLP	AD4 energy E1	AD4 energy E2	AD4 energy E3	AD4 energy E4	AD4Avg Energy	Ludi2 Energy E1	Ludi2 Energy E2	Ludi2 Energy E3	Ludi2 Energy E4	Ludi2Avg Energy
1	CCCCCCC=4C=C3C(O/C=C/C1=C/N(N=C1)C=2C=CC=CC=2)C3=O)=CC=4OC	1840086	100	0,52	-55,83	-8,36	-9,23	-9,19	-8,39	-8,79	-6,87	-9,30	-8,40	-8,14	-8,18
2	[F]C=1C=CC(=CC=1)C4=NC=3/C=C(/NC(=O)C=2C=CC=CC=2)C=CC=3O4	441641	17	0,54	-58,94	-7,49	-7,92	-7,85	-7,41	-7,67	-7,77	-10,71	-7,51	-6,44	-8,11
3	CC=1C=CC=C(C=1)C(=O)NC=3C=CC=2OC(=NC=2C=3)C=4C=CC=CC=4[F]	1081514	6	0,57	-60,16	-7,85	-8,20	-8,41	-7,76	-8,06	-6,94	-10,61	-7,88	-6,94	-8,09
4	CC=1C=CC=C(C=1)C(=O)NC=3C=CC=2OC(=NC=2C=3)C=4C=CC=CC=4	15056	29	0,59	-58,22	-7,91	-8,28	-8,55	-7,73	-8,12	-7,98	-10,28	-7,46	-6,63	-8,09
5	COC=3C=CC(NC(=O)N1CCN(CC1)C=2C=CC([F])=CC=2)=CC=3	162746	85	0,57	-56,20	-6,70	-7,21	-6,67	-7,14	-6,93	-6,15	-10,53	-7,96	-7,39	-8,01
6	CC(C)([H])C=4C=CC(C[N+]3CCN(CC=2C=CC=1OCOC=1C=2)CC3)=CC=4	28818	58	0,64	-56,90	-7,72	-7,34	-8,84	-7,96	-7,97	-7,68	-8,40	-7,49	-8,13	-7,92
7	CC=1C=CC(=CC=1)C(=O)NC=3C=CC=2OC(=NC=2C=3)C=4C=CN=CC=4	1654548	48	0,57	-57,33	-7,45	-7,99	-7,83	-7,58	-7,71	-6,67	-10,79	-7,57	-6,52	-7,89
8	CC=1C=CC(=CC=1)C(=O)NC3=C/C2=NN(N=C2C=C3)C=4C=CC=CC=4	463837	66	0,57	-56,68	-7,80	-8,29	-8,14	-7,71	-7,99	-7,09	-10,80	-7,61	-6,01	-7,88
9	C[C@]([H])(N1CCC(=CC1)C=2C=CC=CC=2)C(=O)NC[C@@]3([H])CCCCC3	4011680	96	0,57	-55,91	-7,87	-8,99	-8,57	-8,63	-8,52	-6,70	-9,63	-6,86	-8,14	-7,83
10	CC=1C=CC=CC=1/C4=N/C=3/C=C(/NC(=O)C=2C=C/C=C(/[F])C=2)C=CC=3O4	453688	59	0,56	-56,87	-7,83	-8,27	-8,14	-7,91	-8,04	-6,52	-10,27	-7,36	-6,89	-7,76
11	[Br]C=1C=NC=C(C=1)C(=O)NC=3C=CC=2OC(=NC=2C=3)C=4C=CC=CC=4	204345	86	0,58	-56,10	-7,95	-8,64	-8,50	-8,10	-8,30	-6,67	-10,73	-6,86	-6,78	-7,76
12	[Br]C=1C=CC=C(C=1)C(=O)NC=3C=CC=2OC(=NC=2C=3)C=4C=CN=CC=4	539663	25	0,58	-58,27	-7,92	-8,28	-8,68	-7,91	-8,20	-6,78	-9,95	-6,83	-7,43	-7,75
13	[Br]C=1C=CC=C(C=1)C(=O)NC=3C=CC=2OC(=NC=2C=3)C=4C=CC=NC=4	539650	65	0,58	-56,69	-7,99	-8,53	-8,89	-7,98	-8,35	-6,44	-8,60	-7,32	-8,25	-7,65
14	CC=1C=CC(=CC=1)C(=O)NC=3C=CC=2OC(=NC=2C=3)C=4C=CC=CC=4	1516651	19	0,57	-58,59	-7,77	-8,22	-7,96	-7,73	-7,92	-5,95	-10,65	-7,00	-6,94	-7,63
15	O=C(CN1CCN(CC1)C(=O)C=2C=CC=CC=2)C3=CNC=4C=CC=CC3=4	1856384	36	0,59	-57,91	-7,98	-7,79	-8,87	-8,25	-8,22	-6,63	-8,55	-7,47	-7,79	-7,61
16	CCOC=4C=CC(NC(=O)CN3C1=CC=CC=2C=CC=C(C1=2)[S]3(=O)=O)=CC=4	2288172	62	0,60	-56,79	-8,59	-8,58	-8,07	-8,36	-8,40	-6,19	-10,27	-6,74	-7,13	-7,58
17	[F]C=1C=CC=C(C=1)C(=O)NC=3C=CC=2OC(=NC=2C=3)C=4C=CC=CC=4	166879	47	0,57	-57,35	-7,56	-7,91	-7,86	-7,40	-7,68	-7,85	-9,65	-6,18	-6,63	-7,58
18	O=C(CCC1([H])CCCC1)N4CC[N+](C/C2=C/NC=3C=CC=CC2=3)CC4	566814	4	0,59	-60,81	-8,50	-7,71	-8,67	-8,13	-8,25	-7,10	-9,86	-7,08	-6,25	-7,57
19	CC=1C=CC=C(C=1)C(=O)NC=3C=CC=2OC(=NC=2C=3)C=4C=CN=CC=4	15079	31	0,59	-58,20	-7,64	-8,07	-8,32	-7,65	-7,92	-6,12	-10,24	-7,54	-6,31	-7,55
20	CCOC(=O)C=1C=CC(=CC=1)N=C2N=CNC3=C2C=NN3C	1666088	15	0,62	-59,10	-6,45	-6,56	-6,66	-6,47	-6,54	-6,04	-11,24	-6,53	-6,38	-7,55
21	O=C(CN1CCN(CC1)C(=O)C=2C=CC(=CC=2)N3C=CC=N3)N4CCOCC4	4370480	95	0,63	-55,92	-7,69	-7,95	-9,32	-8,01	-8,24	-7,47	-7,57	-7,58	-7,40	-7,51
22	CCN(CC)C(=O)C=1C=CC(=CC=1)N(C)[S](=O)(=O)C=2C=CC(OC)=CC=2	4433620	92	0,59	-55,99	-7,35	-7,63	-7,51	-7,44	-7,48	-6,33	-8,77	-7,61	-7,27	-7,49
23	CCOC=1C=CC(=CC=1)N2C[C@@]([H])(CC2=O)C(=O)N3CCC4=CC=CC=C34	3247815	1	0,63	-61,42	-7,87	-8,67	-8,27	-8,23	-8,26	-7,05	-8,75	-7,47	-6,63	-7,48
24	CC=1C=CC=CC=1C(=O)NC=3C=CC=2OC(=NC=2C=3)C=4C=CN=CC=4	539664	44	0,56	-57,54	-7,74	-8,15	-8,23	-7,81	-7,98	-7,00	-9,44	-6,41	-6,78	-7,40
25	[H][C@]4([N+]C/C1=C/NC2=CC=CC=C12)CC[N+](CC=3C=CC=CC=3)CC4	2308121	3	0,63	-61,05	-7,65	-7,46	-8,13	-7,73	-7,74	-6,40	-10,36	-5,93	-6,85	-7,38
26	CC/C4=N/C=3C=CC(OC=2C=CC=1/N=C(/CC)NC=1C=2)=CC=3N4	130913	38	0,59	-57,86	-7,10	-8,10	-8,14	-7,09	-7,61	-5,60	-11,37	-6,71	-5,85	-7,38
27	COC=1C=CC=C(C=1)N4C(=O)[C@@]3([H])N/N=C(/C(=O)C=2C=CC(=CC=2)C(C)(C)C)[C@@]3([H])C4=O	1757351	23	0,46	-58,37	-8,95	-9,17	-9,07	-8,55	-8,94	-7,21	-8,10	-6,40	-7,79	-7,37
28	CCOC(=O)C=1C=CC(=CC=1)N=C2N=CNC3=C2C=NN3C=4C=CC=CC=4	1693420	5	0,53	-60,56	-7,23	-7,72	-7,77	-7,70	-7,61	-6,31	-10,04	-6,61	-6,04	-7,25
29	CC(=O)OC=2C=CC=1C(=O)C(=COC=1C=2C)C3=CN(N=C3)C=4C=CC=CC=4	213602	89	0,57	-56,04	-7,83	-8,32	-7,58	-7,93	-7,92	-6,52	-9,35	-6,83	-6,10	-7,20
30	[F]C=1C=CC(=CC=1)N4N=C3C=CC(NC(=O)C=2C=CC=NC=2)=CC3=N4	517958	88	0,55	-56,04	-7,33	-8,16	-7,52	-7,52	-7,63	-6,44	-9,74	-6,44	-6,16	-7,19
31	COC=4C=CC=3NC2=C(N=CN(CC=1C=C/C=C(/OC)C=1OC)C2=O)C=3C=4	1942623	26	0,56	-58,25	-7,07	-7,30	-6,95	-7,02	-7,09	-6,19	-9,12	-6,22	-7,06	-7,15
32	CC(=O)NC=3C=CC(OC=2C=CC=1/N=C(/C)NC=1C=2)=CC=3	1092527	87	0,56	-56,08	-6,94	-7,02	-8,23	-6,60	-7,20	-6,95	-8,55	-6,78	-6,29	-7,14
33	CC=1C=CC=C(C=1)C(=O)NC=3C=CC=2OC(=NC=2C=3)C=4C=CC=NC=4	15069	61	0,59	-56,83	-7,75	-8,36	-8,84	-7,74	-8,17	-6,57	-7,54	-7,17	-7,01	-7,07
34	CCOC(=O)N3CCN(CC(=O)C1=C(C)NC=2C=CC=CC1=2)CC3	396392	83	0,70	-56,22	-7,37	-7,21	-8,28	-7,17	-7,51	-6,20	-8,36	-6,52	-7,09	-7,04
35	CCOC(=O)[C@@]2([H])CC[N+](CCCCO/C1=C/C=C/C=C1/C)CC2	3030928	84	0,64	-56,21	-6,54	-6,50	-6,88	-6,42	-6,59	-6,76	-7,77	-6,52	-7,12	-7,04
36	CCOC=1C=C(=CC=1)N3C(=O)C[C@@]([H])(CC=2/C=C(/C)C=C(C)C=2)C3=O	96334	18	0,60	-58,65	-7,80	-8,79	-8,32	-7,91	-8,21	-5,86	-7,73	-7,70	-6,60	-6,98
37	CCOC=1C=CC(=CC=1)C2=NC(=NO2)C=4C=C3C=C/C=C(/C)C3=NC=4O	585307	71	0,59	-56,47	-8,01	-8,82	-7,69	-8,20	-8,18	-6,11	-9,38	-6,03	-6,35	-6,97
38	NC=1C=CC=C(C=1)C(=O)NC=3C=CC=2N=C(NC=2C=3)C=4C=CC=NC=4	575907	32	0,55	-58,20	-7,68	-8,15	-8,63	-7,51	-7,99	-6,03	-9,82	-5,92	-6,11	-6,97
39	CCOC=1C=CC(=CC=1)N3C(=O)C[C@@]([H])(CC=2C=C/C=C(/C)C=2)C3=O	96847	2	0,60	-61,21	-7,42	-8,37	-8,77	-7,35	-7,98	-6,71	-7,42	-7,28	-6,46	-6,97
40	C[C@]([H])(OC(=O)[C@@]1([H])CCCCC1)C(=O)NC=2C=CC(NC(C)=O)=CC=2	3441584	72	0,56	-56,45	-7,79	-8,27	-8,16	-7,34	-7,89	-6,89	-7,16	-6,78	-7,05	-6,97
41	NC(=O)C=1C=C[S]C=1NC(=O)CN4C=NC2=C(C=NN2C=3C=CC=CC=3)C4=O	2104819	42	0,56	-57,58	-8,32	-8,01	-8,76	-7,98	-8,27	-6,00	-7,25	-6,29	-7,80	-6,84
42	CCCNC(=O)N1CCC([H])(CC1)C=3C=C2OCOC2=CC=3	3241398	74	0,62	-56,41	-6,94	-7,02	-7,40	-6,99	-7,09	-5,63	-9,33	-6,15	-6,18	-6,82
43	CCOC=1C=CC(=CC=1)N=C2N=CNC3=C2C=NN3C=4C=CC(C)=CC=4	1675205	7	0,52	-60,14	-7,00	-7,59	-7,21	-7,56	-7,34	-5,70	-8,48	-6,41	-6,59	-6,79
44	CCOC=1C=CC(=CC=1)C3=NN(CC(=O)NC=2C(C)=CC=CC=2C)N=N3	1185579	55	0,57	-56,97	-8,07	-7,84	-7,62	-7,85	-7,85	-5,92	-7,58	-6,60	-6,90	-6,75
45	[F]C=4C=C1C(N/C=C1/CCNC(=O)C=2C=C(N=CC=2)N3CCOCC3)=CC=4	5253967	97	0,56	-55,89	-7,78	-7,80	-8,50	-7,71	-7,95	-6,23	-7,34	-6,46	-6,89	-6,73
46	COC=3C=CC(C[C@]1([H])CC(=O)N(C1=O)C=2C=CC(OC)=CC=2)=CC=3	95473	14	0,59	-59,38	-7,27	-8,15	-8,68	-7,34	-7,86	-5,37	-7,32	-7,30	-6,70	-6,67
47	CCOC=1C=CC(=CC=1)N3C(=O)C[C@@]([H])(CC=2C=CC(C)=CC=2)C3=O	95456	12	0,58	-59,50	-7,34	-8,40	-7,11	-7,43	-7,57	-5,88	-6,56	-7,45	-6,49	-6,59
48	COC=3C=CC(NC(=O)C1([H])CCN(CC1)[S](=O)(=O)C=2C=CC=CC=2)=CC=3	909537	57	0,55	-56,90	-8,05	-8,12	-8,33	-7,67	-8,04	-6,55	-7,38	-5,66	-6,63	-6,55
49	CCOC=3C=CC(CN/C2=N/N1C(NC(C)=C(C)C1=O)=N2)=CC=3	773733	11	0,67	-59,52	-7,38	-7,42	-8,40	-7,18	-7,60	-6,33	-7,81	-6,37	-5,65	-6,54
50	C/C4=N/N=C(/CN3C(=O)N[C@@]([H])(C/C1=C/NC2=CC=CC=C12)C3=O)O4	3331268	54	0,63	-57,02	-7,74	-7,77	-8,45	-7,28	-7,81	-6,03	-8,62	-5,93	-5,32	-6,47
51	COCCCNC(=O)C2=C/C=C(/C[S]CC=1C=CC=CC=1[Cl])O2	843870	13	0,61	-59,45	-6,79	-6,82	-6,95	-6,46	-6,76	-5,82	-6,87	-6,75	-6,41	-6,46
52	CCOC=1C=CC(=CC=1)C3=NN(CC(=O)N2CCC[C@@](C)([H])C2)N=N3	1185596	70	0,57	-56,50	-7,30	-7,69	-7,33	-7,16	-7,37	-5,93	-7,34	-6,00	-6,31	-6,40
53	CCOC=1C=CC(=CC=1)N3C(=O)C[C@@]([H])(CC=2C=CC(OC)=CC=2)C3=O	465282	77	0,57	-56,34	-7,15	-8,24	-6,79	-7,37	-7,39	-6,07	-7,13	-6,46	-5,78	-6,36
54	CCCCCC[C@]1([H])CC[C@@]([H])(CC1)C2=NC(=NO2)C=3C=CN=CC=3	796749	22	0,59	-58,41	-7,64	-8,33	-8,60	-7,56	-8,03	-5,35	-7,47	-5,86	-6,71	-6,35
55	CCCNC(=O)CN3C(=O)N[C@@]([H])(C/C1=C/NC=2C=CC=CC1=2)C3=O	2147727	24	0,62	-58,29	-7,13	-7,44	-7,44	-6,75	-7,19	-4,42	-9,97	-5,02	-5,73	-6,28
56	CCOC=2C=CC(OCCC(=O)NC=1[S]C=CC=1C(N)=O)=CC=2	2211919	46	0,62	-57,40	-6,71	-6,97	-7,00	-7,04	-6,93	-5,41	-5,93	-5,33	-8,30	-6,25
57	OC=1C=CC=CC=1/C2=C/C(=NO2)C(=O)NC=4C=CC=3OCOC=3C=4	673190	63	0,62	-56,71	-7,78	-8,07	-7,87	-7,55	-7,82	-5,59	-8,25	-5,07	-5,77	-6,17
58	NC(=O)C=1C=C[S]C=1NC(=O)CN3C=NC2=C/C=C(/[Cl])C=C2C3=O	4361863	27	0,62	-58,24	-7,89	-8,08	-8,49	-7,63	-8,02	-5,35	-7,21	-6,42	-5,63	-6,15
59	COC=3C=CC(CN/C2=N/N1C(NC(C)=CC1=O)=N2)=CC=3	1914329	91	0,69	-55,99	-6,86	-6,59	-8,19	-7,06	-7,18	-5,59	-7,25	-5,97	-5,45	-6,07
60	CCOC(=O)N1CCC([H])(CC1)NC(=O)C2=NNC=3CCCCC2=3	5235271	33	0,68	-58,08	-7,59	-7,91	-7,76	-7,03	-7,57	-5,82	-6,38	-6,25	-5,80	-6,06
61	CCOC=1C=CC(=CC=1)C3=NN(CC(=O)NCC2C=CC=CC=2)N=N3	1185602	99	0,57	-55,86	-7,71	-7,90	-8,19	-7,63	-7,86	-5,82	-6,97	-5,74	-5,70	-6,06
62	O=C(CCN2C=NC1=CC=CC=C1C2=O)N/C4=N/C3=CC=CC=C3N4	5222381	93	0,58	-55,96	-7,72	-7,91	-7,83	-8,03	-7,87	-5,15	-6,40	-4,95	-6,16	-5,67

Figure 2. Structures of the 62 purchased compounds with potential broad spectrum fusion inhibitory activity against dengue virus E proteins.

1

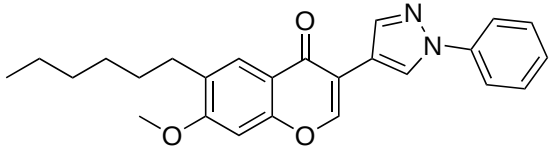

1840086

2

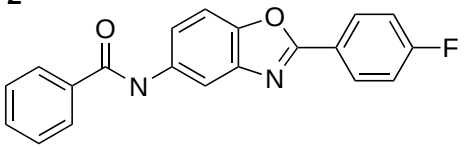

441641

3

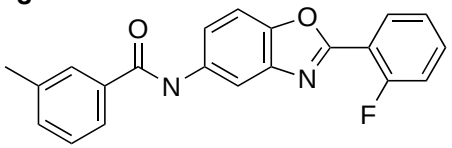

1081514

4

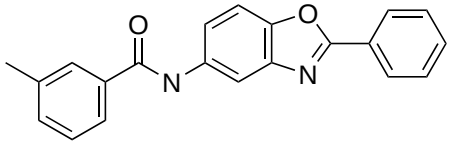

15056

5

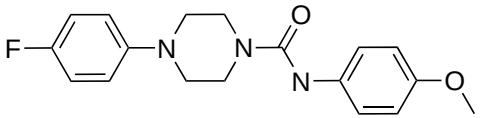

162746

6

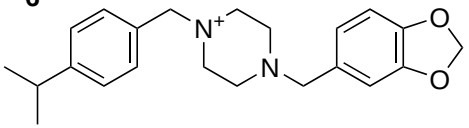

28818

7

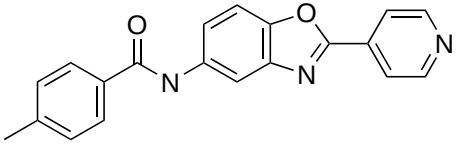

1654548

8

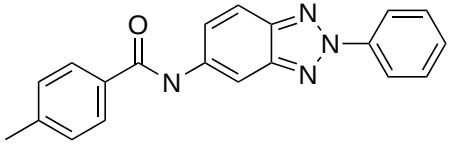

463837

9

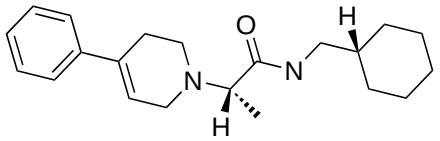

4011680

10

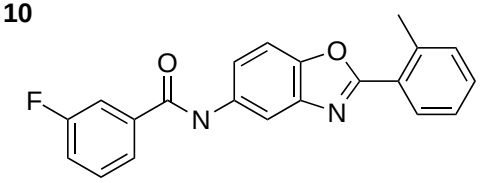

453688

11

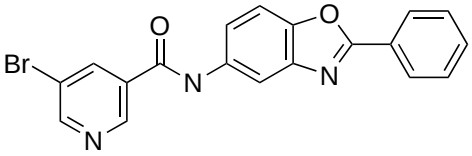

204345

12

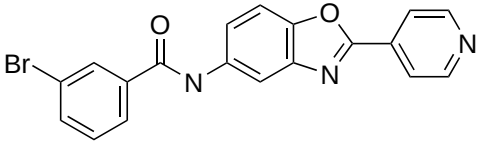

539663

Figure 2. Cont.

13

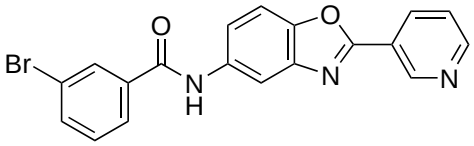

539650

14

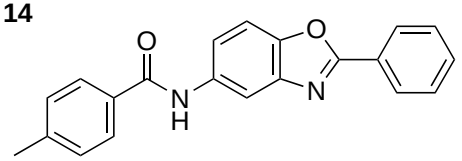

1516651

15

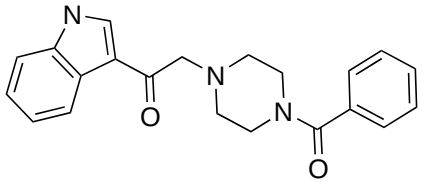

1856384

16

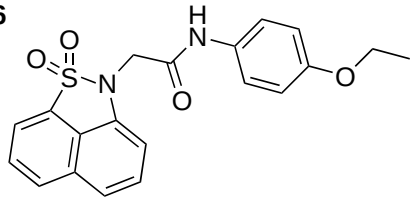

2288172

17

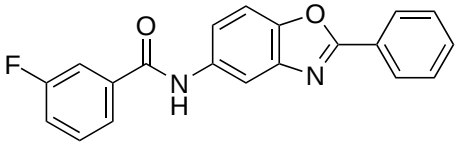

166879

18

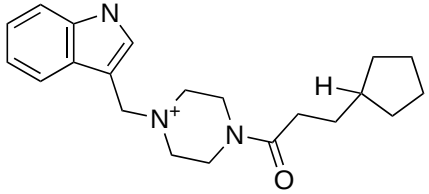

566814

19

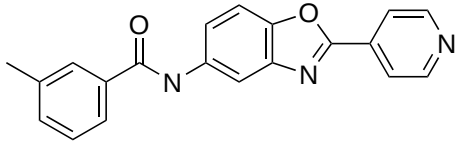

15079

20

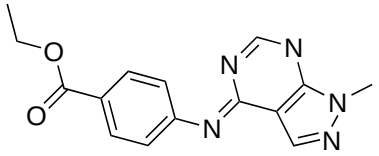

1666088

21

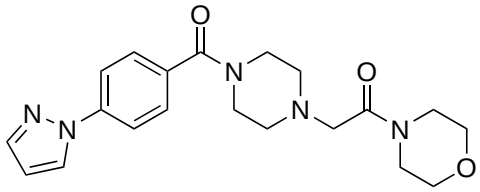

4370480

22

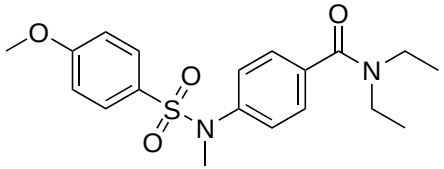

4433620

23

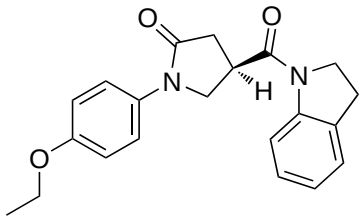

3247815

24

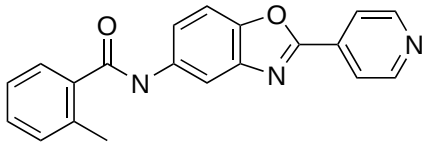

539664

Figure 2. Cont.

25

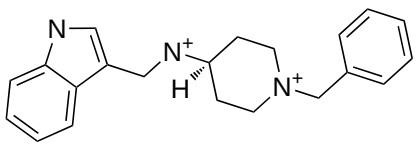

2308121

26

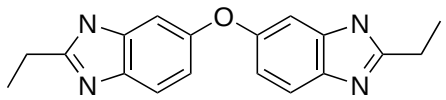

130913

27

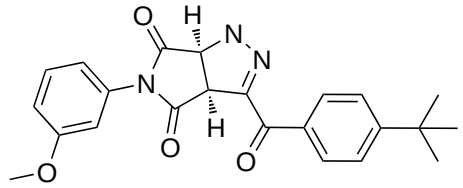

1757351

28

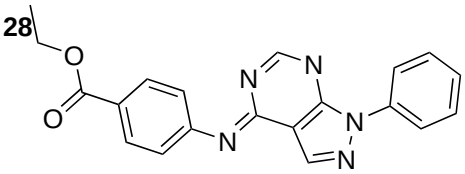

1693420

29

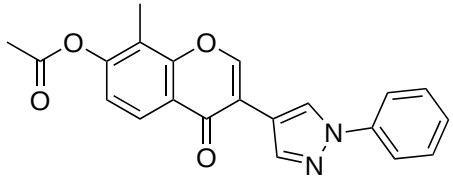

213602

30

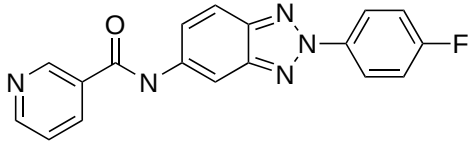

517958

31

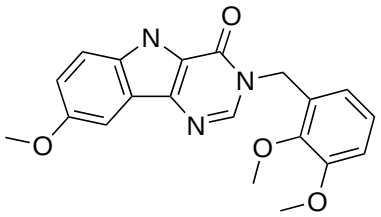

1942623

32

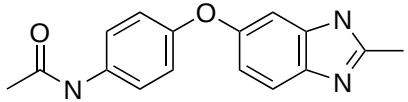

1092527

33

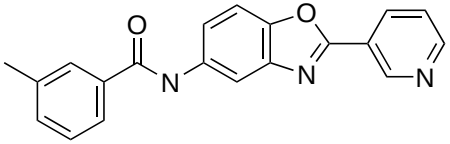

15069

34

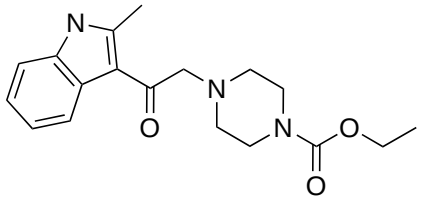

396392

35

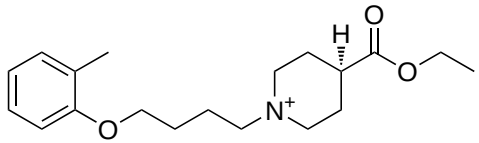

3030928

36

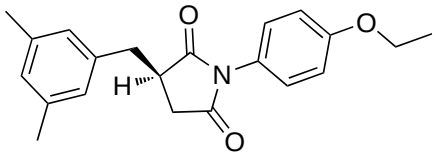

96334

Figure 2. Cont.

37

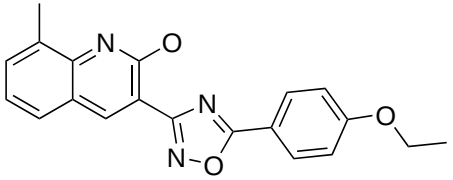

585307

38

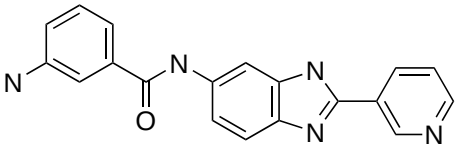

575907

39

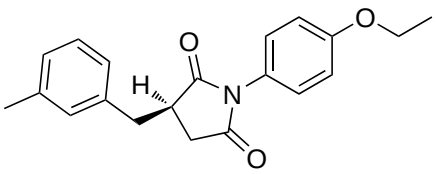

96847

40

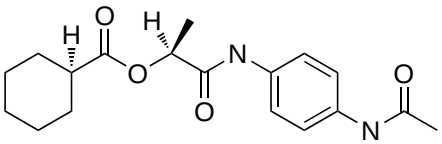

3441584

41

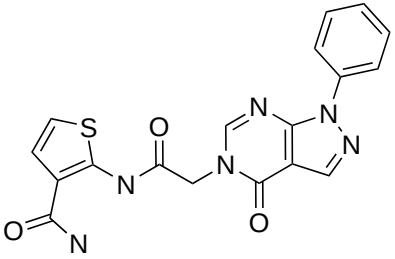

2104819

42

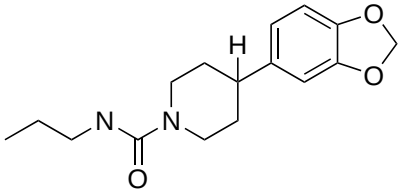

3241398

43

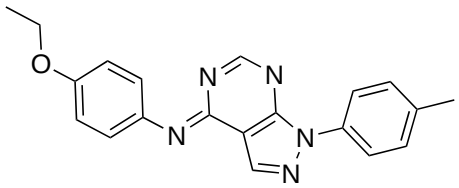

1675205

44

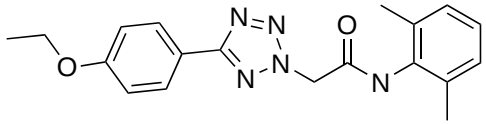

1185579

45

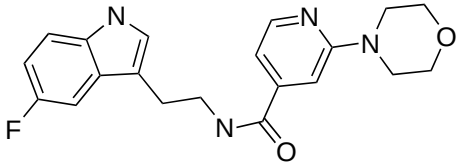

5253967

46

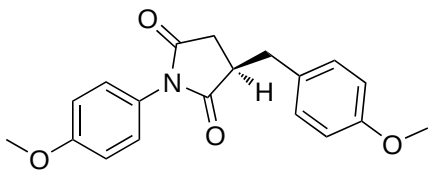

95473

47

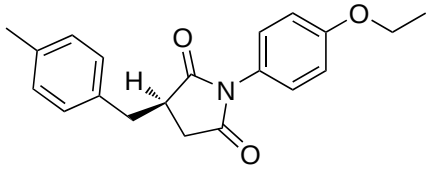

95456

48

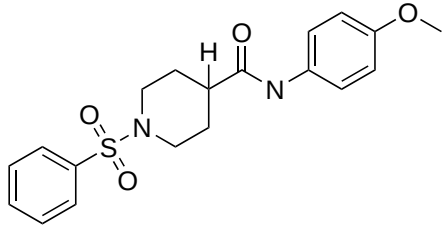

909537

Figure 2. Cont.

49

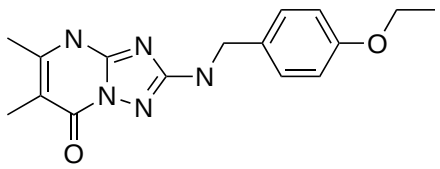

773733

50

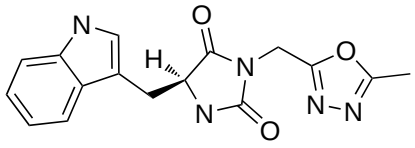

3331268

51

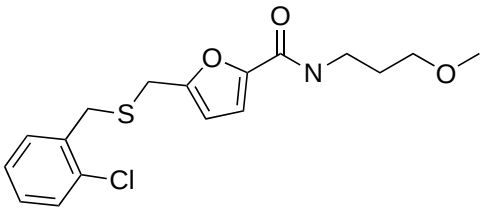

843870

52

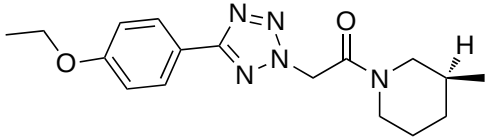

1185596

53

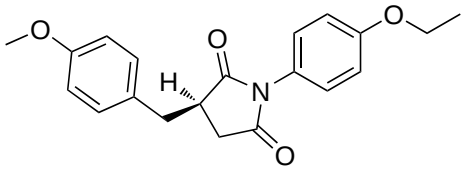

465282

54

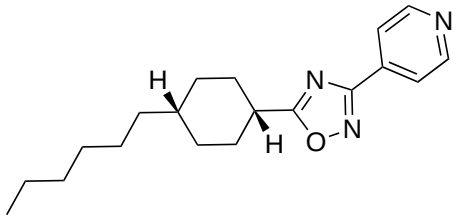

796749

55

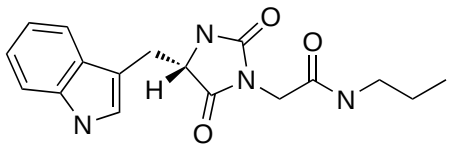

2147727

56

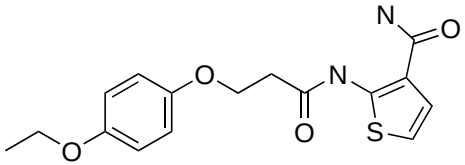

2211919

57

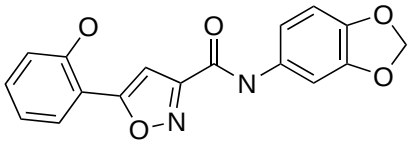

673190

58

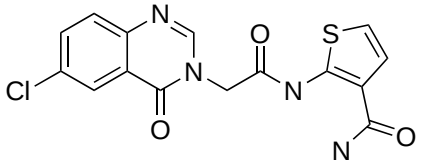

4361863

59

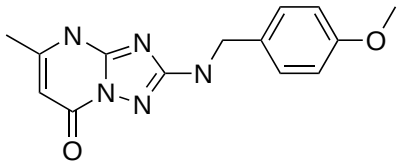

1914329

60

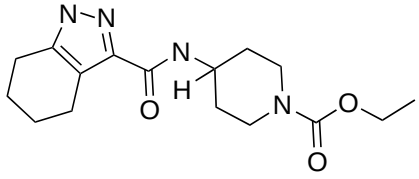

5235271

Figure 2. Cont.

61

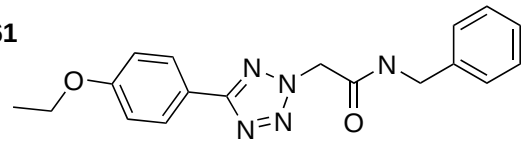

1185602

62

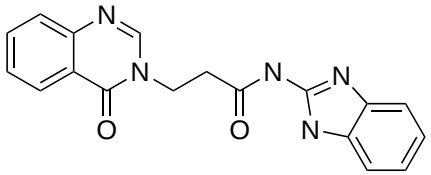

5222381

Oral presentation at the XXXI Reunión Anual de la Sociedad de Bioquímica y Biología Molecular de Chile, 23 to 26 September 2008, Termas de Chillán, Chillán, Chile.

MAPEO COMPARATIVO DE GRUPOS FUNCIONALES EN PROTEÍNAS DE FUSIÓN VIRAL CLASE II

(Comparative functional group mapping of Class II viral fusion proteins)

Lagos, Carlos F.[1]*; Huenchuñir, Patricio[2]; López-Lastra, Marcelo[3] and Pérez-Acle, Tomás[1,4]

[1] Centro de Bioinformática, Facultad de Ciencias Biológicas

[2] Laboratorio de Química Médica, Facultad de Química

[3] Laboratorio de Virología Molecular, Centro de Investigaciones Médicas, Facultad de Medicina, Pontificia Universidad Católica de Chile.

[4] Fundación Ciencia para la Vida.

ABSTRACT

Enveloped viruses infect cells via fusion of the virus membrane with a host cell membrane through viral fusion proteins. Upon appropriate triggering, the fusion protein interacts with the target membrane and undergoes a conformational change that drives the membrane fusion reaction. The structures of the ectodomains of fusion proteins from flaviviruses revealed that although these proteins lack detectable amino acid sequence conservation, their secondary and tertiary structures are remarkably similar. In this work we report the construction of consensus functionality maps for functional group binding in class II fusion proteins. The calculations were done for three flavivirus class II envelope glycoproteins: Dengue virus (DENV), Tick-Borne Encephalitis Virus (TBEV) and West Nile Virus (WNV). The results gave consensus maps that indicate functional groups that are insensitive to the specific protein conformation and the existence of alternative binding sites that could be targeted in the rational design of broad-spectrum inhibitors.

Acknowledgments

CFL is a fellowship of the Fundación Ciencia para la Vida (PFB-16). Funding from grant W81XWH-08-1-0285 USAMRMC is also acknowledged.

Oral presentation at the 5th annual RIB (Red Iberoamericana de Bioinformatica) conference, Pontificia Universidad Catolica, Santiago, Chile, October 15-17, 2008.

Integrated *in silico* tools for drug design

Carlos F. Lagos [1, 2], C. David Pessoa-Mahana [2], Patricio Huenchuñir [2], and Tomás Pérez-Acle[1].

[1] Centre for Bioinformatics CBUC - Faculty of Biological Sciences
[2] Medicinal Chemistry Laboratory MCL - Faculty of Chemistry
P. Universidad Católica de Chile

It is generally recognized that drug discovery and development are very time and resources consuming processes. Current *in silico* strategies for drug design are playing increasingly larger and more important roles in drug discovery and development and are believed to offer means of improved efficiency for both the academic and industrial arena.

In our own academic scenario, we have incorporated several structure and ligand-based techniques into our academic drug discovery programs with promising results. These strategies have been combined to expedite and facilitate hit identification, hit-to-lead selection, optimize the absorption, distribution, metabolism, excretion and toxicity profile and avoid safety issues of a series of ligands designed towards various pharmaceutical targets.

Here we describe the use of computational approaches that include ligand-based drug design (pharmacophore), structure-based drug design (drug-target docking), and quantitative structure–activity and quantitative structure–property relationships to discover new drug candidates from different chemical scaffolds.

Acknowledgements: FONDECYT, United States Army Medical Research and Materiel Command (USARMRC), Fundación Chilena para Biología Celular & Fundación Ciencia para la Vida.

Comparative Functional Group Mapping of Dengue Virus Envelope Proteins.

Carlos F. Lagos[1,*], Patricio Huenchuñir[2], Marcelo López-Lastra[3] and Tomás Pérez-Acle[1,4]
[1]Centre for Bioinformatics CBUC, Faculty of Biological Sciences; [2]Medicinal Chemistry Laboratory MCL, Faculty of Chemistry; [3]Molecular Virology Laboratory MVL, Faculty of Medicine; Pontificia Universidad Católica de Chile. [4]Fundación Ciencia para la Vida.
E-mail: carlos@cbuc.cl

ABSTRACT
Enveloped viruses infect cells via fusion of the virus membrane with a host cell membrane through viral fusion proteins. Upon appropriate triggering, the fusion protein interacts with the target membrane and undergoes a conformational change that drives the membrane fusion reaction. The structures of the ectodomains of fusion proteins from flaviviruses revealed that although these proteins lack detectable amino acid sequence conservation, their secondary and tertiary structures are remarkably similar. In this work we report the construction of consensus functionality maps for functional group binding in class II fusion proteins. The calculations were done for the class II envelope glycoproteins of Dengue virus (DENV) serotypes 1-4. The results gave consensus maps that indicate functional groups that are insensitive to the specific protein conformation and the existence of alternative binding sites that could be targeted in the rational design of broad-spectrum inhibitors.

Acknowledgments
CFL is a fellow of the Fundación Ciencia para la Vida (PFB-16). Funding from grant W81XWH-08-1-0285 USAMRMC is also acknowledged.